

UNIVERSITY OF TARTU  
Faculty of Science and Technology  
Institute of Technology

**Iaroslav Iakubivskyi**  
(Якубівський Ярослав Іванович)

# **Nanosatellite Anatomy Analysis: The Second Generation of ESTCube**

**Master's Thesis (30 ECTS)**  
Robotics and Computer Engineering  
Space Technology

Supervisors:  
Andris Slavinskis, PhD, Tartu Observatory  
Erik Ilbis, MSc

Tartu 2017

## **Nanosatellite Anatomy Analysis: The Second Generation of ESTCube**

### **Abstract:**

Any object that has been launched into orbit has experienced statical and dynamical loads during its travel through the atmosphere. The loads are of random nature and cannot be fully predicted as per real conditions. The structural requirements for ESTCube-2 have been determined as for the worst-case scenario, since the launch vehicle was not known at that stage of the project. A three-unit CubeSat will be subject to high-level sine and random vibration as well as shock response spectrum loading. Before physical testing, structural simulations were made and stresses were analysed in order to confirm the structural reliability and margins. Margins are essential in the design process due to uncertainties in the predicted vibration environment. In addition, the thesis presents the design of primary and secondary structures. As a result of this thesis, a final materials selection, topography optimisation, and manufacturing of the structure will be made. Moreover, the simulation results obtained here will be the subject of comparison with the physical testing results in the later stage of the ESTCube project. ESTCube-2 will be launched in the first half of 2019, and will serve as a testbed for the ESTCube-3 mission in the solar wind environment.

**Keywords:** ESTCube, nanosatellite, structural analysis, simulations, FEMAP

**CERCS:** T210 Mechanical engineering, hydraulics, vacuum technology, vibration acoustic engineering; T320 Space technology.

## **Nanosatelliidi Anatoomia Analüüs: ESTCube Teine Põlvkond**

Igale kosmosesse saadetavale objektile mõjuvad atmosfääri läbides staatilised ja dünaamilised koormused. Nimetatud koormused on juhusliku olemusega ning neid ei ole testimise käigus võimalik täiesti realistlikult reprodutseerida. ESTCube-2 nõuded struktuurile püstitati halvima võimaliku juhu jaoks, kuna käesoleva töö tegemise ajaks ei olnud kasutatav kanderakett veel selgunud. Kolmeühikuline kuupsatelliit kogeb stardil suure võimusega harmoonilisi ja juhuslikke vibratsioone ning ka šokile iseloomulikke koormusi. Enne füüsilise satelliidi testimist simuleeriti satelliidi struktuuri käitumist koormuste mõjul ning muutuste püsimist etteantud vahemikes.

**Teadusvaldkondade ja -erialade klassifikaator:** T210 Masinaehitus, hüdraulika, vaakumtehnoloogia, vibratsioonakustiline tehnoloogia; T320 Kosmosetehnoloogia.

## TABLE OF CONTENTS

<b>LIST OF FIGURES</b>	<b>5</b>
<b>LIST OF TABLES</b>	<b>7</b>
<b>ACRONYMS AND ABBREVIATIONS</b>	<b>8</b>
<b>1. INTRODUCTION</b>	<b>10</b>
<b>2. THEORETICAL BACKGROUND</b>	<b>12</b>
2.1. Acoustic environment	13
2.2. Space mission habitat	14
2.3. Dynamic analysis for single-degree-of-freedom (SDOF)	16
2.4. Stress and strain	17
2.5. Modes of vibration	18
2.6. Structural reliability	19
2.7. Finite element analysis	20
<b>3. MISSION OVERVIEW</b>	<b>21</b>
<b>4. STRUCTURE REQUIREMENTS</b>	<b>23</b>
<b>5. DESIGN DESCRIPTION</b>	<b>24</b>
<b>6. FINITE ELEMENT ANALYSIS MODEL</b>	<b>27</b>
6.1. Simulation environment and model description	27
6.1.1. Software	27
6.1.2. Units	27
6.1.3. Model description	27
6.1.4. Bar elements	28
6.1.5. Mass elements	28
6.1.6. Mesh properties	30
6.1.7. Boundary conditions	31
6.1.7.1. Constraints	31
6.1.7.2. Loads	31
6.2. Materials	32
<b>7. STRUCTURAL ANALYSIS RESULTS</b>	<b>33</b>
7.1. Model check	33

7.1.1. Mass properties	33
7.1.2. Strain Energy and Stiffness Max Ratio Check	33
7.1.3. Free-free check	33
7.1.4. Static load verification	33
7.2. Modal analysis	34
7.3. High-level sine vibration	37
7.3.1. High-level sine vibration in the X-direction	38
7.3.2. High-level sine vibration in the Y-direction	40
7.3.3. High-level sine vibration in the Z-direction	43
7.3.4. High-level sine vibration conclusions	45
7.4. Random vibration	47
7.4.1. Random vibration in the X-direction	47
7.4.2. Random vibration in the Y-direction	51
7.4.3. Random vibration in the Z-direction	55
7.4.4. Random vibration analysis conclusions	59
<b>8. CONCLUSIONS</b>	<b>61</b>
8.1 Future work	62
<b>ACKNOWLEDGMENTS</b>	<b>63</b>
<b>REFERENCES</b>	<b>64</b>
<b>Non-exclusive licence to reproduce thesis</b>	<b>66</b>
<b>Appendix A Mechanical mathematical model requirements</b>	<b>67</b>
<b>Appendix B FEA model description</b>	<b>68</b>



## **LIST OF FIGURES**

Figure 1. Nanosatellites by type

Figure 2. General view of power spectral density

Figure 3. Space environment as the function of altitude

Figure 4a. Plasma brake concept for gravity stabilised tether

Figure 4b. Upcoming large constellations

Figure 5. ESTCube-2 structural requirements

Figure 6a. ESTCube-2 exploded view on the left. Structural elements on the right

Figure 6b. ESTCube-2 mock-up

Figure 7. The ESTCube-2 planar model

Figure 8a. Bar elements

Figure 8b. Mass elements

Figure 9. Mesh model

Figure 10. Participation factors for 300 modes

Figure 11. Von Mises stress for HS vibration in X direction

Figure 12. High-level sine vibration in X-direction. Acceleration graphs for various surfaces

Figure 13. Von Mises stress for HS vibration in X direction

Figure 14. High-level sine vibration in Y-direction. Acceleration graphs for various surfaces

Figure 15. Von Mises stress for HS vibration in Z direction

Figure 16. High-level sine vibration in Z-direction. Acceleration graphs for various surfaces

Figure 17a. Von Mises stress for random vibration in X direction for the entire satellite

Figure 17b. Von Mises stress for random vibration in X direction for the Y-plus U-frame on the bus attachment side

Figure 17c. Von Mises stress for random vibration in X direction for the EO bottom plate

Figure 18a, b. Random vibration accelerations in logarithmic scale in X-direction. Acceleration graphs for various surfaces

Figure 19a. Von Mises stress for random vibration in Y direction for the entire satellite

Figure 19b. Von Mises stress for random vibration in Y direction for the Y-plus U-frame on the bus attachment side

Figure 19c. Von Mises stress for random vibration in Y direction for the EO bottom plate

Figure 19d. Von Mises stress for random vibration in Y direction for the Z-plus payload motor PCB

Figure 20a, b. Random vibration accelerations in logarithmic scale in Y-direction.

Acceleration graphs for various surfaces

Figure 21a. Von Mises stress for random vibration in Z direction for the entire satellite

Figure 21b. Von Mises stress for random vibration in Z direction for the Y-plus U-frame on the bus attachment side

Figure 21c. Von Mises stress for random vibration in Z direction for the EO bottom plate

Figure 21d. Von Mises stress for random vibration in Z direction for the bus PCB

Figure 22a, b. Random vibration accelerations in logarithmic scale in Z-direction.

Acceleration graphs for various surfaces

## **LIST OF TABLES**

Table 1. Units

Table 2. High-level sine profile

Table 3. Random vibration test profile

Table 4. Materials properties

Table 5. FEA mass properties

Table 6. Modal analysis results

Table 7. High-level sine vibration in X direction results

Table 8. HS vibration in Y direction results

Table 9. HS vibration in Z direction results

Table 10. High-level stresses for aluminium group margin of safety

Table 11. High-level stresses for FR4 group margin of safety

Table 12. Random vibration in X direction results

Table 13. Random vibration in Y direction results

Table 14. Random vibration in Z direction results

Table 15. Random stresses for aluminium group margin of safety

Table 16. Random stresses for FR4 group margin of safety

## ACRONYMS AND ABBREVIATIONS

Al	Aluminium
AA	Aluminium alloy
AOCS	Attitude and orbit control subsystem
ASD	Acceleration spectral density
ATOX	Atomic oxygen
CAD	Computer-aided design
COM	Communication subsystem
CoG	Center of gravity
CoM	Center of mass
EO	Earth observation
EPS	Electric power subsystem
E-sail	Electric solar wind sail
EMC	Electromagnetic compatibility
ESD	Electrostatic discharge
EM	Engineering model
ESA	European Space Agency
FEA	Finite element analysis
FPGA	Field-programmable gate array
FH	Flight hardware
GEO	Geosynchronous orbit
CG	Gold gas
HW	Hardware
HS	High-level sine
HSCOM	High-speed communication
IFA	Inverted-F antenna
LV	Launch vehicle
LEO	Low Earth orbit
MoS	Margin of safety
MEO	Medium Earth orbit

OBCS	On-board computer subsystem
PSD	Power spectral density
PCB	Printed circuit board
PDF	Probability density function
PR	Public relations
RF	Radio frequency
RW	Reaction wheel
SDOF	Single-degree-of freedom
SPL	Sound pressure level
SS	Stainless steel
ST	Star tracker
STR	Structure subsystem
Ti	Titanium
UHF	Ultra-high frequency
VHF	Very high frequency

## 1. INTRODUCTION

*The main aim behind the structural analysis is to predict and understand potential problems in the structural design – not colonise numbers!*

The first man-made object that was launched into space was the Sputnik-1 satellite [1] in 1957. That was fascinating and charming for all humankind and escalated the Space Race [2], consequently developing technologies and bringing attention to space science around the globe. Space became more accessible and open not just for governmental space agencies and huge companies, but for universities and other educational institutions in recent years. Technologies and devices have a tendency of becoming smaller in size and more powerful in performance (an ideal example is the smartphone industry). A similar development has occurred in small satellite design, they have decreased in size as well as becoming more standard in their build-up. This trend was introduced by the California Polytechnic State University and Stanford University as CubeSat in 1999. It is a cubic-shape satellite identified by the number of units. One unit, more commonly known as 1U, is a cube with a volume equivalent to the one litre and a side-length of 10 cm. By merging a few cubes on top of each other, the variety of sizes increases (1U, 2U, 3U, 6U...). Satellites can be categorised by their mass. The one with a mass below 1 kg is a picosatellite, which is very often a 1U CubeSat (by default the mass of each unit should not exceed 1.33 kg), or a PocketQube (0.25U). The majority of launched or built CubeSats consist of nanosatellites with a mass of 1-10 kg, shown in Figure 1, as per March 14th 2017 [3]. Aforementioned majority is a 3U CubeSats with a nominal mass limitation equivalent to 4 kg, however depending on the deployer (mechanical interface between the CubeSat and the launch vehicle (LV)) the mass can be higher. As in the case of ISIPOD, the maximum allowable mass for 3U is 6 kg [4]. A spacecraft with a mass range from 10 to 100 kg is a microsatellite, below 1 kg a picosatellite, and below 0.1 kg a femtosatellite. The smallest publicly-known femtosatellite is KickSat, a 3.5 by 3.5 cm single printed circuit board (PCB) with microprocessor, gyroscope, magnetometer, radio with antennas, and solar cells [5].

As with any piece of hardware (HW), a satellite needs a structure for holding it together or deploying into the orbit as per case of KickSat. Moreover, the development process for space structures is somewhat similar to the ground-application one with much more strict requirements and constraints. Development process initiates with the list of requirements and ends up with the product delivering for LV integration; it consists of designing, verification, manufacturing, and testing. Design means developing requirements, identifying options, doing analysis and trade studies, and defining a product in enough detail so one can build it [7, p.1]. For the ground applications, one also considers the outer look (how it looks like and how it feels like), however, for the space mission the main target

in designing is functionality under certain requirements (some exceptions exist for public relations (PR) purposes). Hence, the structure has to be cost-effective which means obtaining high performance, reliability, and confidence for spent money, considering not only knowns but also variables and uncertainties [7, p.1].

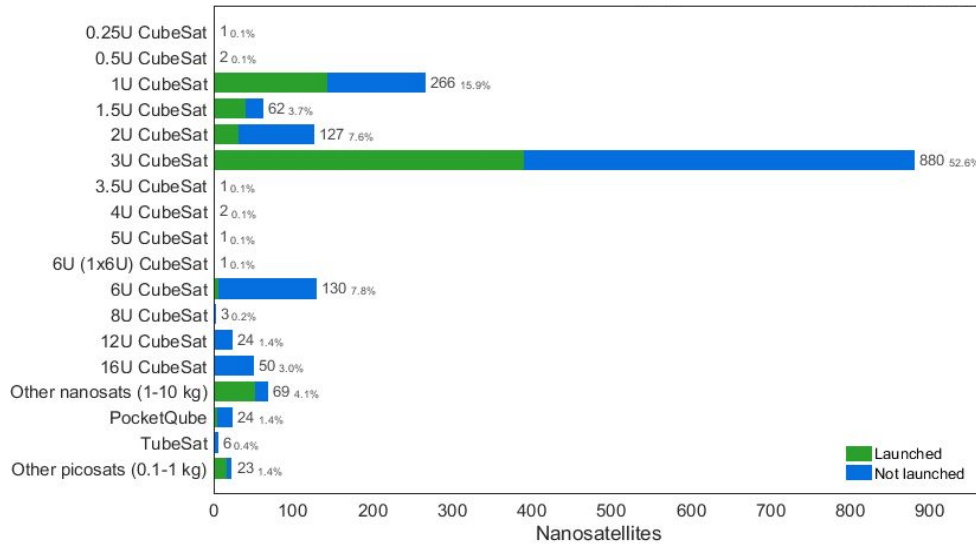


Figure 1. Nanosatellites by type

In the particular case the satellite consists of payloads (which conduct scientific and technologic demonstration and performance) and subsystems or satellite bus (which operates the spacecraft). The structure supports the payload and spacecraft subsystems with enough strength and stiffness to preclude any failure (rupture, collapse, or detrimental deformation) that may keep them from working successfully [7, p.23]. Key requirements consist of functional (what must be done), operational (how well it must be done), and constraints (limit the available sources, schedule, or physical characteristics) [7, p.26]. The risk has to be evaluated and if the elimination is not feasible due to constraints in terms of time, cost, or schedule shift, then one has to accept the certain probability of failure or damage. In addition, the level of risk has to be evaluated with its influence on the entire mission – will it cause full mission failure or just minor element deformation that does not affect the mission success. Any risk evaluation starts with the estimation of failure probability and resolving consequence of that failure.

This thesis focuses on simulations of structural vibration and predictions of stress in the ESTCube-2 structure. It evaluates the margin of safety for various structural parts and ability of structure to withstand launching loads. In addition, it describes mechanical design and the challenges occurred during last two years in the satellite development that have influenced structural modifications of a 3U CubeSat built by the ESTCube team.

## 2. THEORETICAL BACKGROUND

An object with the main purpose of being functional outside Earth's atmosphere has to be able to survive harsh environments. Survival implies a guaranteed functionality of subcomponents after and during the exposure to certain loads. Moreover, the degradation level of chosen materials should stay under settled limits. The environments in question are the ground, launching environment, and space conditions. In order to understand and predict loads that are created by various natures, the life-cycle events of spacecraft have to be understood from cradle to grave. However, for nanosatellites, ground loading will be skipped in the scope of this work due to decreased complexity. The main focus is on the launching loads (e.g. vibration); the space and ground environments will be introduced in this section as well.

The origin of structural loads is either static (constant) or dynamic (varying with time). Each can be external (e.g. uniformed mass loading in the case of static; sound pressure in the case of dynamic) or self-contained (e.g. pressure of stored propellant in the case of static; mass loading during vibration in the case of dynamic). The spacecraft load events are manufacturing, transporting, integration, testing, ground handling, prelaunch preparation, launch, separation, in-orbit operation, and if applicable, reentry and landing. Among them, the launch loads are the most critical for the structure; they are not under the control, thus the structure has to be designed to tolerate them. Most importantly, the launch cycle has to be understood.

**Launch** starts with lift-off, once the booster engines are ignited, and ends with the payload separation by putting it to its final orbit. The LV typically consists of stages: when the propellant of first stage is used, it pyrotechnically separates and the second stage engines ignite. This process repeats and depends on the number of stages. Aforementioned events create loads with different nature. Deterministic loads can be predicted as a function of time, others – estimated statistically as random loads. But load factors do not adequately represent dynamic loading that varies with the location and time; in order to predict structural responses to low- and high-frequency vibration, dynamic loads analyses are required [7, p.41]. It is challenging to predict a single- and multiple-event load with its critical and dangerous parts and then combine predicted loads in the way as they occurred in reality. Loads can be relatively steady state or periodic. Relatively constant acceleration (rocket engine burns) of LV causing structural vibration that is referenced in this thesis as high-level sine (HS) vibration originated from the sinusoidal loads. The sound pressure waves are causing sound loads better known as acoustics; these waves occur at various frequencies, consequently the structure vibrates randomly and is referenced in this thesis as random vibration. The pyrotechnical separation of stages causing high-frequency and



intensity short time vibration is better known as a pyrotechnic shock.

During the altitude rise, the transient air pressure, or overpressure forces, are acting on the LV. The main complexity behind these forces is an unsymmetric profile, meaning the pressure waves are hitting the vehicle from one side and create pressure differences, consequently shaking the LV and payload(s). Acoustic pressure waves typically occur between 20 and 10 000 Hz. In order to decrease the sound pressure effect, acoustic blankets might be attached to the fairings inner walls.

## 2.1. Acoustic environment

An **acoustic environment** is presented in terms of sound pressure level (SPL) which is the root-mean-square (rmc) pressure within a frequency band, expressed in decibels. The rmc pressure  $P(f)$  at frequency  $f$  is [7, p.44]

$$P(f) = \sqrt{\frac{1}{T} \int_0^T p(f, t)^2 dt} \quad (1)$$

where  $T$  is duration,  $p(f, t)$  is the pressure at time  $t$  of acoustic waves within a selected frequency band whose centered frequency is  $f$ . A decibel (dB) is the logarithm of a ratio

$$SPL(f) = 20 \cdot \log \frac{P(f)}{P_{ref}} \quad (2)$$

where  $P_{ref}$  is a reference value set to  $2 \cdot 10^{-5} Pa$ .

The structure vibrates randomly in response to the aforementioned sound pressure. Random vibration is typically characterized by the power spectral density (PSD) curve shown in Figure 2 (modified from [7, p.46]). Depending on the desired parameters the term “power” represents acceleration, displacement, stress, etc. In the particular case is an acceleration PSD function, also referenced as an acceleration spectral density (ASD). The ASD at the frequency  $f$ , which is designated  $W(f)$ , is the mean-square acceleration within selected frequency band (whose center is  $f$ ) divided by the bandwidth, typically represented in  $g^2/Hz$  [7, p.46]. It is plotted on log-log paper and as a general rule is covering frequencies from 20 Hz to 2000 Hz. The ASD function for the ESTCube-2 satellite is given in [Section 6.1.7.2](#).

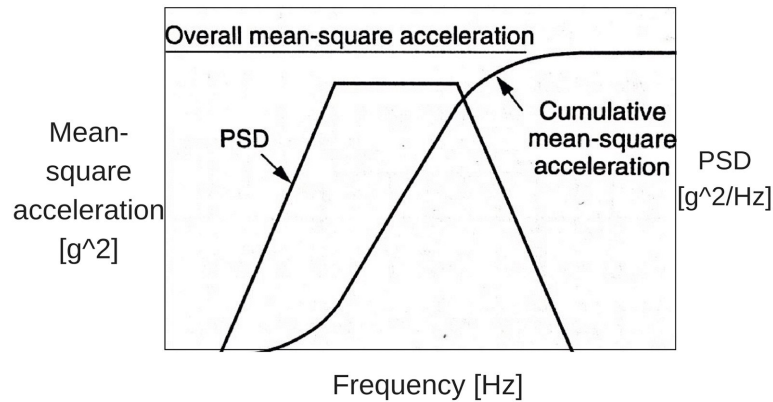


Figure 2. General view of power spectral density.

To understand PSD, one should imagine the device capable of measuring the acceleration with an adjustable frequency limit (starting from zero and increase by steps). By plotting values, one will obtain the curve as in Figure

2. The term “density” implies taking the derivative of the function of cumulative mean-square acceleration, or finding its slope. The slope indicates frequency at which vibration is the most intense [7, p. 46].

Moreover, large loads are addressed from the point when the vehicle crosses the speed of sound (transonic period). The loads are created by shock waves originated from changes in the aerodynamic pressure. Another pyrotechnical event is a fairing separation. The fairing’s main function is to protect the payload from the air pressure and to provide an aerodynamic shape for the LV. Once the rocket reaches the altitude where the atmospheric density is low enough to not influence the LV – an explosive fairing separation takes place that consequently creates shock for the structure.

## 2.2. Space mission habitat

After the satellite reaches required orbit it will be exposed to other harmful habitats in the near-Earth space environment. The list consists of, but is not limited to, vacuum, thermal radiation, charged-particles radiation, neutral atomic and molecular particles, micrometeorites and space debris, magnetic fields, and gravitational fields [7, p.61]. Various sources are influencing the man-made objects as a function of orbit (Figure 3), where LEO is a low Earth orbit (160-2000 km), MEO is a medium Earth orbit (2000-35000 km), and GEO is a geosynchronous orbit (35876 km).

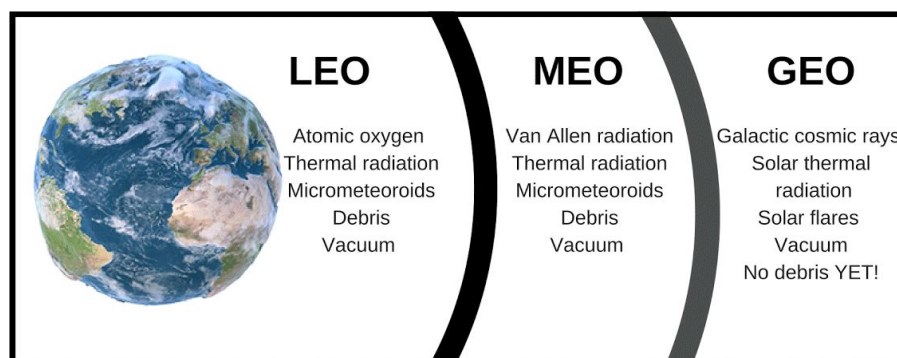


Figure 3. Space environment as the function of altitude

The term **vacuum** describes extremely low pressure in space. A vacuum has various effects on the structure. In vacuum, polymer-based materials (thermal insulators, adhesives, and the matrices for advanced composites) release substances in a gaseous form [7, p.63]. The substance is one of an organic origin or absorbed nitrogen, oxygen, and carbon dioxide on the ground. Moreover, the material has issues with water desorption that was absorbed by the material during on-ground processes. The aforementioned effects may degrade certain properties of material and might cause condensation on critical surfaces (lenses, mirrors, and sensors). Another effect is the internal pressure of sealed structures that was assembled at the ambient Earth pressure.

**Thermal radiation** is mainly a reference to direct solar flux ( $1309\text{--}1400\text{ W/m}^2$ ) which means intensity of radiation, planetary albedo (global annual average is 0.3) which originates from the reflected solar flux, planetary emission flux ( $189\text{--}262\text{ W/m}^2$ ), and the satellite electronics' infrared thermal emission. This results in a nonuniform heating of spacecraft which causes materials (especially with various thermal expansion coefficients) to expand differently, resulting in structural stresses. In addition, certain components require a precise operation temperature range (e.g. batteries, propellant tanks). The solution is to implement an active (requires power) and/or a passive (materials and coatings) thermal control system.

**Charged-particle radiation** is a high flux of energetic particles. The major sources are *trapped radiation* (Van Allen belt) which contains electrons and protons in the MEO, *galactic cosmic radiation* which contains 90% of protons and 10% of helium nuclei in the GEO and further, and *solar radiation* which is largely continuous solar wind (electrons, protons, and helium nuclei low in energy) and solar flares (high energetic protons and heavy ions) [7, p.69]. The radiation has a negative effect on the electronics and may cause damages or failure. There is no way to predict or to be protected against galactic cosmic radiation, thus electronics have to tolerate it. Against trapped and solar radiations, shieldings are implemented. The structure of the satellite can act as a radiation shield as well. For instance, in order to keep the total radiation dose below  $10\text{e}4$  rads per year at 4000 km, the required thickness of aluminium is 9 mm [7, p.71].

LEO contains relatively stable atomic and molecular particles. When the spacecraft moves at orbital hypervelocity, its surface is struck by particles that cause material recession. The most damaging is atomic oxygen (ATOX) [8]; among other impactors are  $N_2$ ,  $O_2$ ,  $Ar$ ,  $He$ ,  $H$ . The erosion process and rates rely on the material's composition. The most damaging are polymer based materials, while the impact on metals is not that significant, especially on aluminium (Al) which is commonly used for space structures due to its low density, radiation shielding capabilities, and manufacturability. For instance, an exposed Al surface to ATOX at an altitude of 500

km has an erosion rate of  $7.6 \times 10^{-6}$  mm/year, however the same parameters applied to silver results in the erosion rate of 0.22 mm/year [9].

**Micrometeoroids and space debris** can have a fatal impact on the spacecraft structure at the orbital hypervelocity due to impacts (if the size of impactor is large enough). One can implement shielding againsts smaller objects. In addition, thermal blankets decrease the impact of small objects. The ESTCube-2 satellite will test plasma brake deorbiting technologies that are potentially capable of decreasing the amount of debris in the near and far future ([Section 3](#)).

### 2.3. Dynamic analysis for single-degree-of-freedom (SDOF)

This subsection gives an overview to the behavior of a single-degree-of freedom (SDOF) system that has been influenced by force. A forcing function describes how applied force varies with time and frequency, so that time-domain or frequency-domain analysis can be implemented.

A system driven by harmonic or sinusoidal force can be represented as the sum of individual harmonic forces. Simple harmonic loading can be represented as [7, p. 107]

$$F(t) = F_0 \sin(\Omega t) \quad (3)$$

where  $F(t)$  is the applied force at time  $t$ ,  $F_0$  is the maximum applied force, and  $\Omega$  is the frequency of the input force in radians per second.

For base-drive systems, response acceleration,  $a_{rms}$ , to random vibration will be equal

$$a_{rms} = \sqrt{\int_0^{\infty} [|H(f)|^2 W_a(f)] df} \quad (4)$$

where  $f$  is a frequency,  $|H(f)|$  is the gain of complex transfer function,  $W_a(f)$  is defined over frequency range.

For an SDOF, or any mounted structure, the one can approximate (4) with Miles' equation shown in Equation (7) [7, p.121]:

$$a_{rms} = \sqrt{\frac{\pi f_n W_a(f_n)}{4\zeta}} \quad (5)$$

where  $a_{rms}$  is the rms response acceleration,  $f_n$  is natural frequencies,  $W_a(f_n)$  is the input acceleration PSD at frequency  $f_n$ ,  $\zeta$  is a damping factor that is described in Equation (6), and  $Q$  is the quality factor (transability), equal to  $1/2 \zeta$ .

$$\zeta = \frac{\ln(x_1) - \ln(x_2)}{2\pi n} \quad (6)$$

where  $x_1$ ,  $x_2$  are measured peak displacements for two vibrational cycles,  $x_2$  is at a

later time than  $x_1$ , and  $n$  is the number of vibrating cycles separating  $x_1$  and  $x_2$ .

John W. Miles' equation is used to calculate rmc acceleration for an SDOF [10]:

$$G_{rms} = \sqrt{\frac{\pi}{2} f_n Q W_a(f_n)}, \quad (7)$$

Miles' equation can also be used to predict other responses such as stress or acceleration. The example of displacement is shown in Equation (8).

$$Y_{rms} = \sqrt{\frac{Q W_a(f_n)}{32\pi^3 (f_n)^3}} \quad (8)$$

Equation (5) can be also approximated to Equation (9)

$$a_{rmc} = \sqrt{\frac{\pi Q f_n W_a(f_n)}{2}} \quad (9)$$

The value of rmc itself is not sufficient for design. For about 68% of loading time the absolute value of acceleration will be less than the rmc value; the peak response will be higher [7, p. 122].

As it was already mentioned, other response parameters can be achieved by using Fourier transform function and Equation (4). This can be applied to the displacement,

$$W_x(f) = \frac{1}{(2\pi f)^4} W_a(f) \quad (10)$$

By substituting Equations (8) and (10) the rms displacement occurs

$$x_{rms} = \sqrt{\frac{\pi f_n W_x(f_n)}{4\zeta}} = \sqrt{\frac{W_a(f_n)}{64\pi^3 \zeta f_n^3}} = \sqrt{\frac{Q W_a(f_n)}{32\pi^3 f_n^3}} \quad (11)$$

The displacement response for a multiple-DOF system becomes much more complex.

## 2.4. Stress and strain

If the force that acts on a surface is divided by the area that is perpendicular to force, one will obtain the value of normal stress  $\sigma$  typically measured in [Pa]. The resulting displacement to unit length characterizes dimensionless strain  $\varepsilon$ . The ratio between stress and strain gives modulus of elasticity, presented in Equation (12), better known as Hooke's Law, which makes it a measure of a material's stiffness.

$$E = \frac{\sigma}{\varepsilon} \quad (12)$$

Ultimate tensile strength is the highest tensile strength a material can withstand. Once a material is under the elastic limit, it returns to its original shape after unloading. Otherwise the material becomes plastic – it yields, remaining residual strain after the load is removed. A ductile material deforms plastically (elongation) before rupturing [7,

p.127]. Yield, ultimate stresses, and elongation are the basis for determining a material's strength under certain loads. Under tension a material thins, thus negative ratio of lateral to axial strain is used; it is better known as Poisson's ratio.

Similarly to stiffness, strength can be predicted considering the geometry. The amount of a single-event load that a structure can withstand is called strength. Failure can be rupture or collapse (ultimate failure), excessive permanent deformation (yield or joint shift), or excessive elastic deformation [7, p.227]. Strength analysis is implemented in order to design a structure that will not experience failure (avoid potential issues). It is based on a limit load; a factor of safety is a multiplier for limit load in order to reduce the risk of failure. It will be further discussed in [Section 2.6](#). The main problems behind structure failure are instability (disturbances under compression causing buckling), yielding or rupturing at joints, and fatigue.

## 2.5. Modes of vibration

A mode shape is the deformed shape of a structure that is vibrating at one of its natural frequencies. Modes can be either normal or complex. If structural dumping is relatively light or evenly distributed, as is usually the case, the structure's modes will essentially be normal modes of vibration, in which all points in the structure reach their peaks of displacements simultaneously for a given mode. For an undamped freely vibrating structure in one of its normal modes, the ratio of displacements at any two points in the structure is constant at all time [7, p. 184].

The equation for estimating the approximate fundamental frequency of any uniform thin plate, regardless of shape or boundary conditions, was first introduced by Jones in 1975 [12]:

$$f_n = \frac{1.2769}{2\pi} \sqrt{\frac{g}{\delta_{max}}} \approx 0.2 \sqrt{\frac{g}{\delta_{max}}} \quad (13)$$

where  $f_n$  is the fundamental frequency,  $g$  is the acceleration of Earth's gravity, and  $\delta_{max}$  is the peak displacement of the plate under its own weight.

If dumping is taken into consideration, the shape of each structural mode becomes more complex. As in the complex mode, the displacements of points do not peak at the same time; imaginary numbers are required in order to describe their shapes. All structures are lightly damped.

A powerful way to predict a structure's mode shapes, natural frequencies, and its responses to applied forces is to model the structure with discrete DOFs, thus breaking a complex structure into simple structures that are easier to analyze by applying matrix mathematics in order to obtain solutions. This approach is called finite element analysis (FEA). [7, p.188]

## 2.6. Structural reliability

In order to design a reliable structure, the loads that are implemented during the verification process and testing campaign have to be marginally higher than expected ones. However, the loads are very often unpredictable as they vary with every launch, even if the LV remains the same. The loads can be predicted acknowledging historical records (by implementing a mathematical model to data or having a large number of recorded launches (which does not exist considering rocket science history) in the form of histogram until some level of probability for the next launch (typically it should be kept within 99.9%). A mathematical model of the histogram for continuous random variables is typically represented as a probability density function (PDF). It is useful as data points approach infinity. PDFs can be of the common bell shape, such as for normal (Gaussian) distribution, or they can be asymmetrical, or skewed, as in the Rayleigh distribution [7, p.344].

In the structural design, the term confidence is associated with the probability. For instance, one can make a statement that the design load has the probability of 99.9% with 97% confidence. It can be interpreted as there is 97% probability that the design load will not be exceeded more than 0.1% of the launches (considering the histogram).

Typically, the factor of safety (multiplier) for the space unmanned mission is 1.25 (in order to avoid permanent structure deformation that might jeopardize the mission), for the manned mission this value should be at least 1.4.

Many programs have recognised the need to select a probability goal for limit loads and to combine loads statistically from different random sources to achieve it. The most commonly used mathematical model for load variation is the Gaussian distribution. Typically used limit load has the value equal to the mean plus standard deviations (99.87% probability) which is referred as a  $3\sigma$  load [7, p.350]. Such probability is implemented in the current analysis.

Very often the terms **factor of safety** and **margin of safety** (MoS) are conflated. These are two different terms: the first means multiplier for a limit load in order to decrease the chance of failure; the second is the measure of extra strength above certain criteria. The equation for the MoS in the scope of this project is shown in Equation (14).

$$MoS = \frac{\sigma_{allowable}}{1.25 \cdot \sigma_{design}} - 1 \quad (14)$$

where  $\sigma_{allowable}$  is the allowable load or stress (material's properties), the coefficient 1.25 is a factor of safety, and  $\sigma_{design}$  is the design load or stress. The strength analysis obtains a positive result in the case that the MoS is greater than or equal to zero.

Unfortunately, very often the MoS is seen as an authoritative measure of structural integrity. Managers, customers, and reviewers tend to see the MoS without getting

into details behind the value. Engineers quickly realised it and tended to manipulate some inputs in order to receive positive MoS. This is **the main purpose of this thesis**: to describe analysis in enough detail and make an appropriate conclusion afterwards. **Negative values** of the MoS **do not** mean that the structure will fail, it means that the structure has failed the strength analysis under certain criterias. If some elements obtain negative values of the MoS, the costs in terms of schedule shifts and financial aspects have to be reconsidered for the redesign. In some cases, the risk has to be accepted by allowing designed parts with an MoS below zero.

## 2.7. Finite element analysis

The finite element analysis (FEA) is implemented to structure that is broken up into elements, whose shapes are described by nodes. Each element has its own mass and stiffness matrices with as many rows and columns as there are DOFs (between one and six – three translations and three rotations). Thus in total the model has six DOFs times the number of nodes minus any grounded (constrained) DOF(s).

Structural FEA includes static and dynamic solutions. In static analysis, time is not a variable. In dynamic analysis, we apply loads as a function of time. Reactions, displacements, loads, and stresses are solved by software for either analysis. In addition one can obtain mass properties, natural frequencies, mode shapes, and element strain-energy contributions [7, p. 578].

The analysis is based on nodal DOFs, thus all forces, displacements, or any other inputs must be applied on nodes. Typically, the software allows applying force per surface area and element's faces exposed to it. The distributed loads can have various shape.

For a static solution one has to constrain (ground) enough DOF(s) for static equilibrium. Otherwise, the stiffness matrix will be singular which means it will not be inverted, and the solution sequence will not run [7, p. 580]. In the scope of current work we ground the reference node, which is located remotely from the body with attachments to the satellite rails.

An engineer decides the level of details for the FEA model and mesh density based on results that are expected after the analysis. In some cases, one would like to take advantage of symmetry subsequently reducing the size of model and computational time in order to execute analysis.

Every analysis has to be validated in order to ensure fidelity of results. **Analysis validation** typically entails checking the model and analysis method [7, p. 592]. Among validation points are mass properties, free-free check, stiffness check, and one-g load factors. [Appendix A](#) describes requirements for the FEA validation.



### 3. MISSION OVERVIEW

The Estonian Student Satellite Foundation is a non-profit organisation that is in a charge of building the series of ESTCube spacecraft. The first Estonian satellite was ESTCube-1 launched from Guiana Space Center on May 7th, 2013 at 5:05 EEST on-board European Space Agency (ESA) Vega LV [6]. The second generation is ESTCube-2 which is in active development at the moment; the engineering model will be ready by summer 2017. The ESTCube-2 satellite is mainly built by students from the University of Tartu (Estonia) with the professional support and advising from Tartu Observatory (Estonia). The mission analysis and list of partners are presented in the current section.

ESTCube-2 is a 3U nanosatellite with its main mission to test an electric solar wind sail (E-sail) [13] and plasma brake (deorbiting technologies) in LEO [14]. The E-sail is a propellantless propulsion based on the Coulomb force – an interaction between the positively charged body (long, thin tether(s) in our particular case) and the solar wind plasma. The ESTCube-2 satellite will evaluate thrust in LEO [15] by changes in the satellite spinning rate that is required for tether deployment [16]. Moreover, the ESTCube-2 will serve as a testbed for ESTCube-3 with its main mission to test the E-sail in its native heritage – solar wind.

Another application related to the Coulomb force is a plasma brake shown in Figure 4a. The plasma brake is an end-of-life disposal technique for objects in the LEO. The infamous space debris issue was regulated with a limit in the orbital post-mission lifetime of 25 years or 30 years after launch for all satellites in the LEO [17]. The problem behind already existing debris are upcoming large constellations shown in Figure 4b. The probable collisions at orbital hypervelocities (over 3 km/s) will cause defragmentation which will consequently result in an enormous escalation of small objects, better known as the Kessler syndrome, which will disable access to LEO if the escalated problem is ignored.

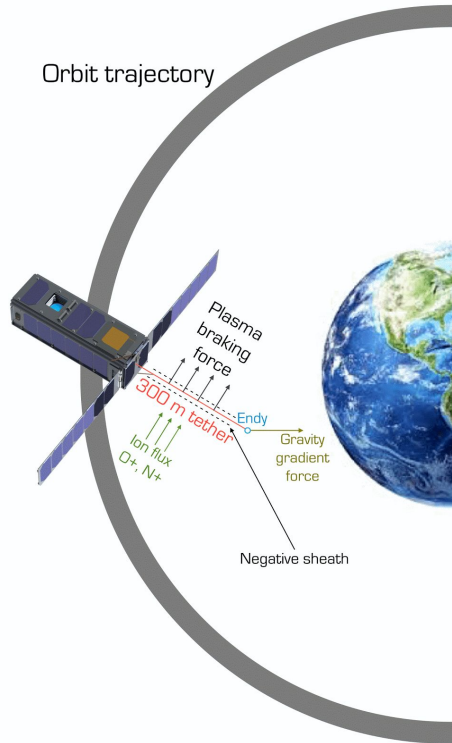


Figure 4a. Plasma brake concept for the gravity-stabilised tether

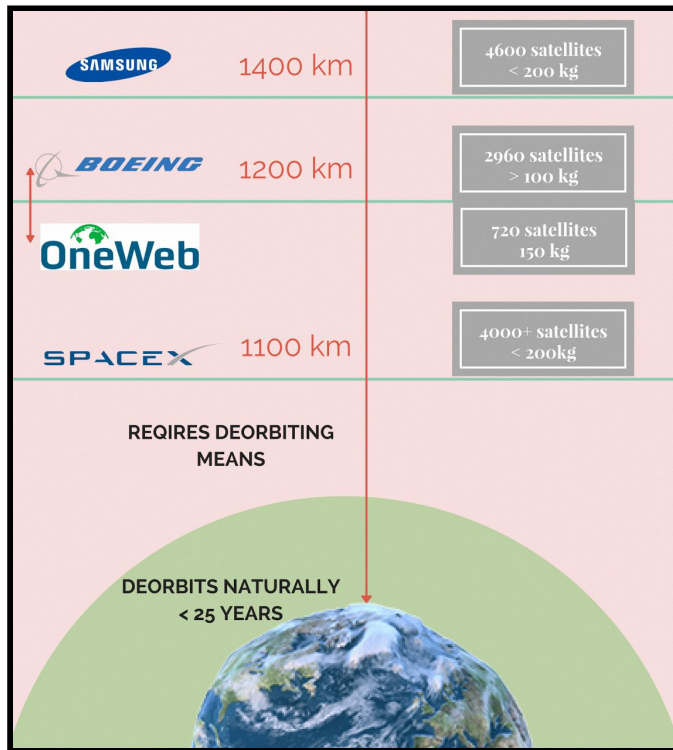


Figure 4b. Upcoming large constellations

A three hundred meters tether, charged up to 1 kV ( $\sim 3$ W of power consumption) on-board ESTCube-2 is expected to decrease the spacecraft's orbital altitude from 700 km to 500 km in six months [18].

The satellite bus has been designed to be as small as possible ( $\sim 0.6$ U) in order to host more payloads. A highly integrated bus is under development and currently consists of typical satellite subsystems, three reaction wheels (RWs), a star tracker (ST), and batteries [15]. The ESTCube-2 subsystems include attitude and orbit control (AOCS), electric power subsystem (EPS), communication (COM), on-board computer (OBCS), star tracker (ST), and structure (STR).

Among other payloads are C-band communication developed by Ventspils University College in Latvia, gold gas (CG) propulsion provided by GOMSpace (former NanoSpace) in Sweden, a corrosion resistance coating experiment developed by the Laboratory of Thin Film Technology and Captain Corrosion OÜ in Estonia, and a dual-optical payload developed by ESTSat OÜ in Estonia. The tether payload (E-sail and plasma brake) is developed by the Finnish Meteorological Institute in Finland.

## 4. STRUCTURE REQUIREMENTS

Structure requirements have been made based on the ECSS-E-30 Part 2 [19] and on the requirements and constraints provided by the payloads and partner institutions. The diagram with requirements is shown in Figure 5 (Color identify how critical the requirement is, red being the most critical). The mechanical mathematical model requirements for FEA validation are described in [Appendix A](#).

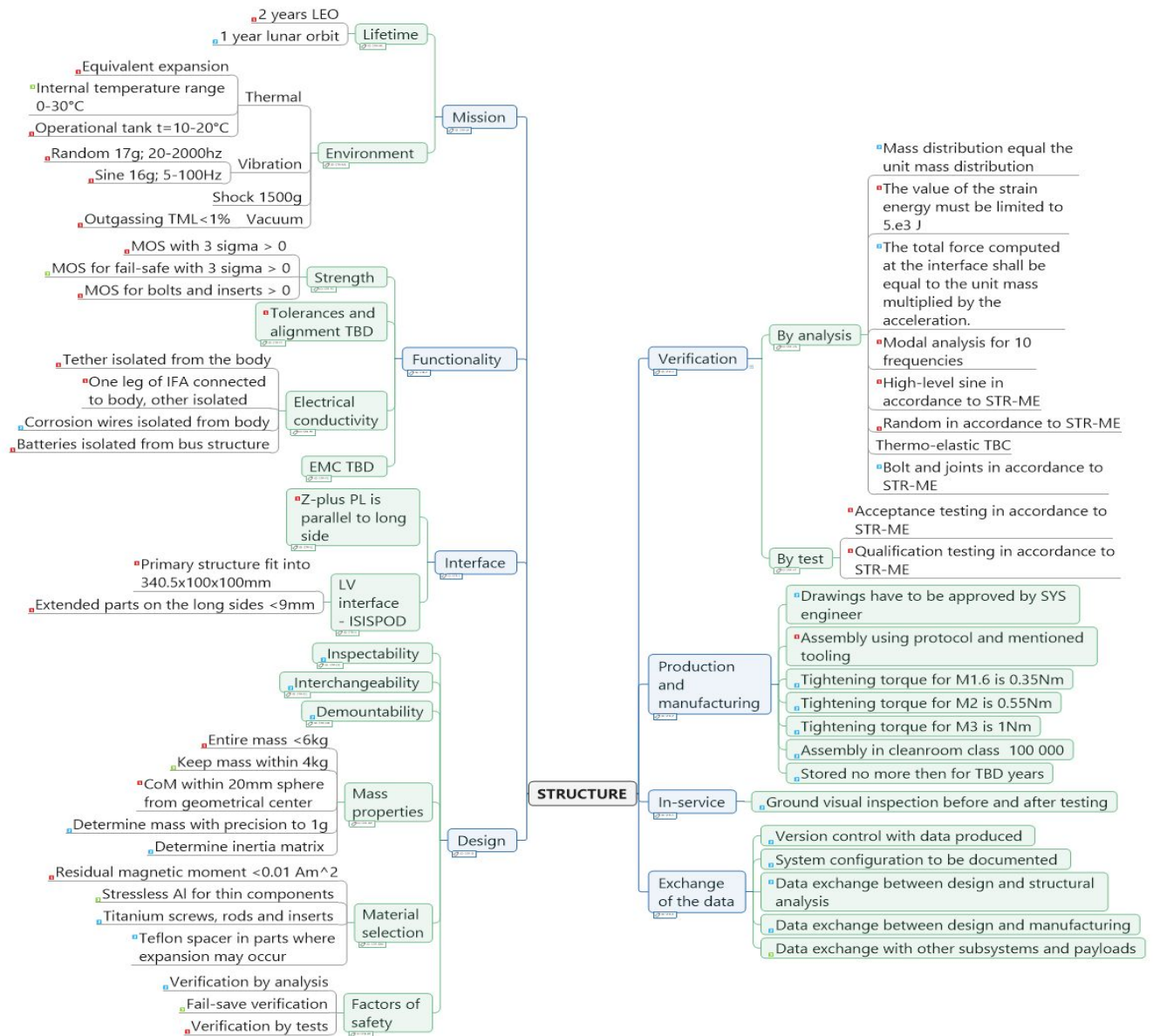


Figure 5. ESTCube-2 structure requirements

## 5. DESIGN DESCRIPTION

While the market offers satisfactory off-the-shelf CubeSat structures for educational projects [20], a custom design provides more flexible and efficient usage of the satellite space. Moreover, custom design brings a lot of flexibility for thermal control design and radiation shielding especially for the nanosatellite outside the magnetosphere. The ESTCube-1 satellite had a monoblock structure (frame) that was complicated and costly in terms of manufacturing; it also caused some problems with assembly and disassembly [21]. Thus the preference for a multi-frame solution. Monoblock structure milling means the processing (in terms of manufacturing) of a solid block of material; typically it is aluminium 6061 or 7075 in the case of CubeSats [22]. The multi-frame solution is based on manufacturing separate sides (flat frames) from plate-material and fastening them together by technical means (e.g. bolts). In addition, such structure is more flexible in designing and manufacturing. Moreover, it prevents constant structure deformation under the stress that might be concentrated at some parts (where an attachment bolt will fail, consequently decreasing the stress on the structure). However, the assembly process and alignment become more challenging, and may take some extra volume and mass.

Materials with non-ferromagnetic properties must be used in the structure, if possible to implement, which is the requirement derived from altitude and orbit control system (AOCS). In the ESTCube-1 mission ferromagnetic parts of the satellite caused a constant magnetic dipole moment and therefore a torque with respect to Earth's magnetic field [21]. Thus, the goal is to avoid aforementioned problems in future developments. For this reason, in the current design all bolts and inserts should be made out of titanium (Ti) alloys. Exceptions are springs for deployable panels and inverted-F antenna (IFA) deployment mechanism; springs will be made out of stainless steel (SS) with relatively low magnetic properties, which mainly depends on the metals added to alloys. Considering the cost of Ti elements (e.g. Ti M2 screw is in the order of 20-40 times more expensive than SS), they will be implemented just for the flight hardware (FH), while for the engineering model (EM) SS or equivalent analogues will be used.

The ESTCube-2 structure consists of primary and secondary structures. The primary structure consists of two identical U-shaped frames, Z-plus and Z-minus short-side panels; X-plus, X-minus, Y-plus and Y-minus long-side panels, and bus structure. The names are associated with the position of parts in relation to the origin coordinate system. An exploded view of the satellite with the coordinate system is shown in Figure 6a. The computer-aided design (CAD) renderings have been performed in the SolidWorks 2016/2017 software.

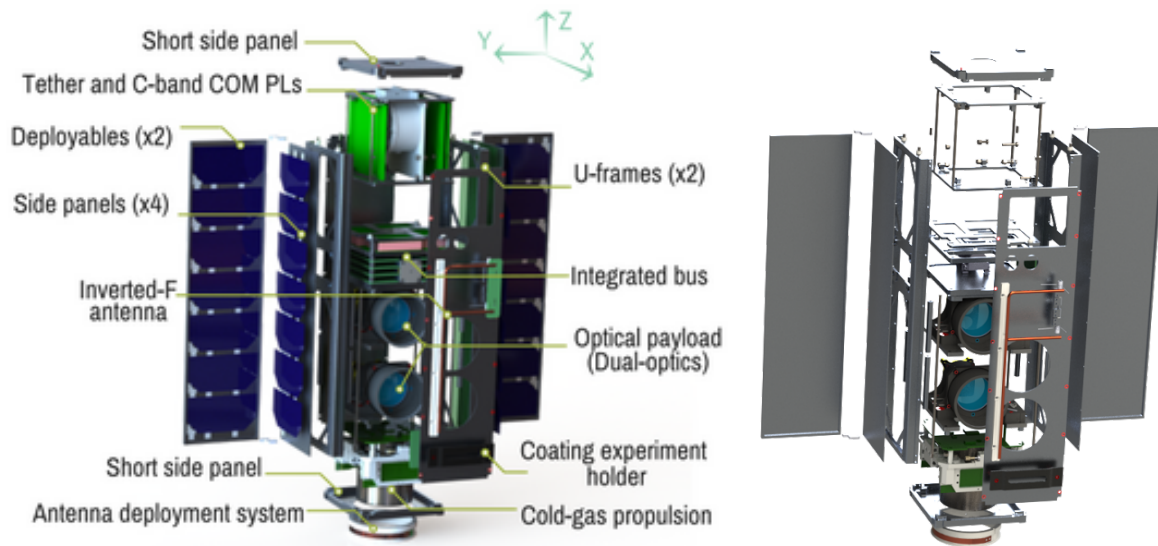


Figure 6a. ESTCube-2 exploded view on the left. Structural elements on the right

The main satellite bus is a fully integrated independent unit that occupies approximately a half of CubeSat unit. It consists of the spacecraft main subsystems, three RWs, ST and batteries. Additionally it has magnetic coils integrated to the side panels and Sun sensors on the external surfaces of the side panels. It is designed in a way that extra battery pack(s) can be added on top, if required by the power budget. RWs and batteries are off-the-shelf products, all the rest are developed in-house.

The secondary structure consists of two internal blocks and two external deployable solar panels. Two payload blocks surround the bus from Z-plus and Z-minus sides respectively.

The Z-plus payload block will be inserted from the top as a single unit and will consist of two payloads, provided by partners mentioned in [Section 3](#). It is the tether payload by the Finnish Meteorological Institute and the C-band communication payload. The tether payload consists of two Printed Circuit Boards (PCBs): motor and high-voltage supply. The high-speed communication will be equipped with two PCBs as well. The entire Z-plus block will have physical connection with the satellite bus structure and will be pressed by conical inserts that are interconnected with the Z-plus short-side cover plate and top-top bus plate (see [Appendix B](#) for the detailed FEA model).

Another block of payloads is located in the Z-minus direction and is integrated from the bottom as a single unit. It consists of optical instrument and propulsion. The optical instrument is two separate cameras that shares PC104 corner rods with CG propulsion. Cameras are developed in-house. The CG propulsion is delivered by GOMSpace (former NanoSpace), that contains 100 g of butane pressurised tank. It is required for the spinning outside Earth's magnetosphere in combination with RWs.

Spinning can be achieved by magnetic coils in the LEO [23]. The thrust direction, employing four nozzles, will differ for the second and third generations: Z-minus for ESTCube-2; Y-plus and Y-minus (two in each direction) for ESTCube-3.

The satellite also will have magnetic coils integrated into side panels, ultra high frequency (UHF) inverted-F antenna (IFA) deployed from X-plus side panel, and very high frequency (VHF) whip antenna that is wrapped around the “tuna can” space and deployed approximately in the same direction as IFA towards the X-plus direction. X-plus will face the Earth during the satellite operation which is the requirement from the optical instruments. In addition, the patch antenna (C-band communication) and wire holder (coating experiment) are mounted on the X-plus side. Antennas should be parallel to Earth.

The ESTCube-2 mock-up has been outsourced to Salibar<sup>1</sup> (Estonia) under the author’s supervision and is shown in Figure 6b. It will be used for the public outreach and press release in order to popularise space technology and science.

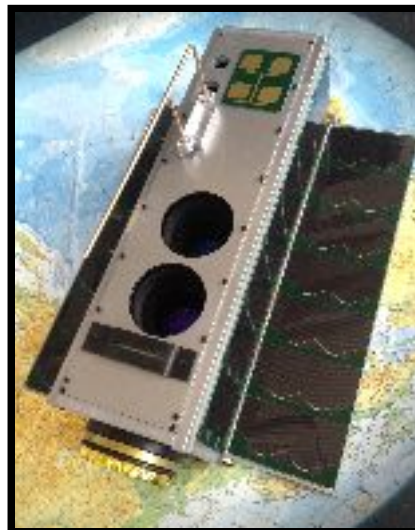


*Figure 6b. ESTCube-2 mock-up*

---

<sup>1</sup> Company web page, <http://www.salibar.ee> (visited 9.05.2017)



## 6. FINITE ELEMENT ANALYSIS MODEL

### 6.1. Simulation environment and model description

#### 6.1.1. Software

The CAD model has been made in the SolidWorks 2016/2017 software. The pre- and post-processing has been made in FEMAP v11.2.2 from Siemens PLM and the associated solver is NX Nastran v10.2 from Siemens PLM.

#### 6.1.2. Units

Unless otherwise specified the following default FEM units have been adopted:

Table 1. Units

Length	$m$
Mass	$kg$
Force	$N$
Momentum	$Nm$
Material density	$kg/m^3$
Young's module	$N/m^2$
Stress	$N/m^2$
Displacement	$m$
Acceleration	$m/s^2$
Frequency	$Hz$

#### 6.1.3. Model description

Based on the 3D model, the geometry has experienced modifications by adopting planar (flat) surfaces instead of volumetric ones. This approach is commonly implemented in the FEMAP environment due to the execution time and model complexity. The thicknesses with appropriate shell elements representation are described in [Appendix B](#) and implemented in the meshing properties described in [Section 6.1.6](#). Figure 7 shows the planar model.

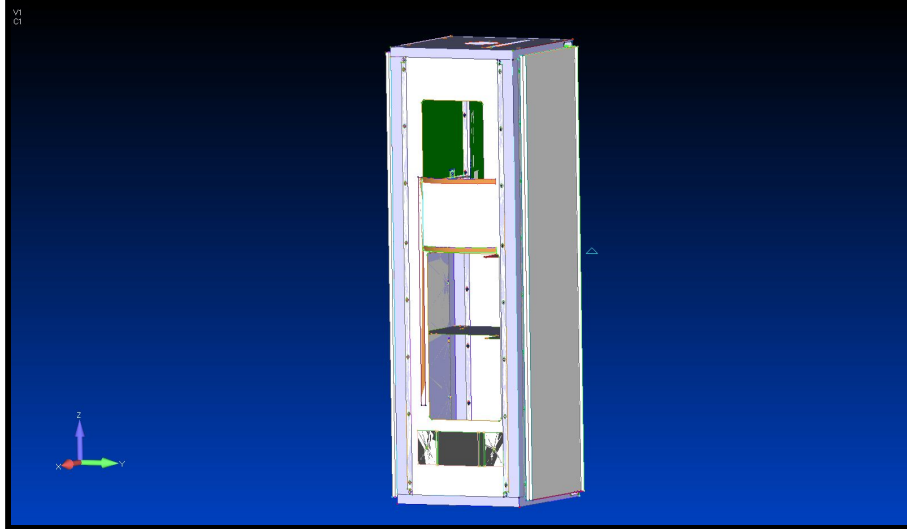


Figure 7. The ESTCube-2 planar model

#### 6.1.4. Bar elements

Rigid elements in the appropriate holes were created in order to simulate the satellite bolts and inserts. The central node of required shell element was connected with a bar that simulates the bolt. The visual representation of bar elements is shown in Figure 8a.

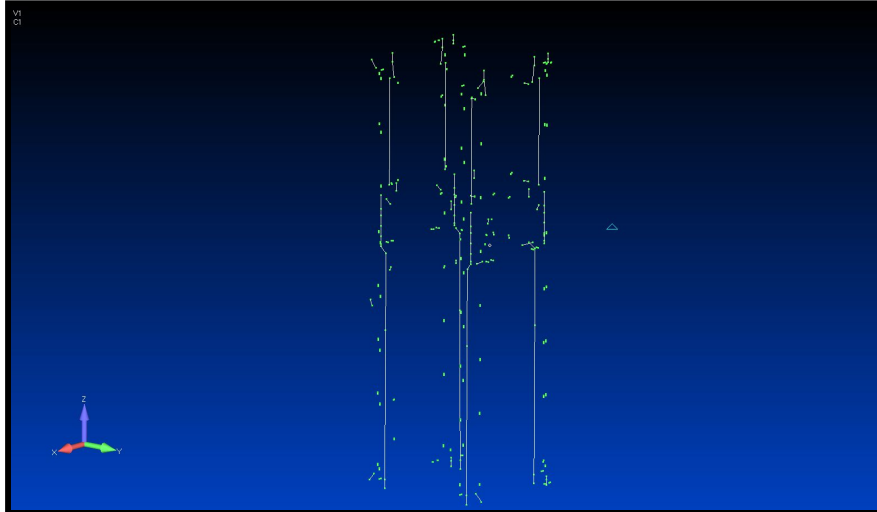


Figure 8a. Bar elements

#### 6.1.5. Mass elements

Some of the structural elements have been represented as mass points created in their CoMs with appropriate masses. Such an approach has been implemented in order to simplify the structural analysis for parts that are developed and already tested, or ones that are too complex and require separate analysis (e.g. EO imager).



The list of simplified parts:

- The E-sail reel/spool (150 g + 100 g of the non-structural distributed mass on the PCB);
- Three RWs (25 g each – RW210<sup>2</sup>);
- ST optics (100 g including margins for the electronics and additional structural elements);
- Two EO imagers (420 g each without bottom plate, considering an initial mass and shortened/smaller baffle option);
- CG propulsion (580 g wet mass, taking into account, that the 50 g butane tank option is 380 g, adding 140 g to the extruded tank structure and 60 g extra grams for the butane).

In addition, non-structural masses were implemented to the elements that are simulating the electronics components or other small components, that are irrelevant for the structural analysis:

- All PCBs have approximately  $100 \pm 10$  g of a non-structural masses, the exception is HSCOM PCBs: an RF board is 30 g and FPGA one is around 47 g.
- Batteries<sup>3</sup> are represented as non-structural masses on the bus top and top-top plates, 77 g to each (the single battery is 38.5 g; four are in total);
- Solar cells<sup>4</sup> (1.5 g each, considering that the density equivalent to  $50 \text{ mg/cm}^2$ , the single cell area is  $30.18 \text{ cm}^2$ ). Each deployable panels mass is around 90 g (including glue and wires by the conservative estimate) and 50 g on X-minus, Y-plus, and Y-minus sides.

The total satellite mass (~4.9 kg) may differ slightly after manufacturing, since the mass estimate in the design includes maximum allowable margins. Mass elements are shown in Figure 8b.

---

<sup>2</sup> Product description, <http://hyperiontechnologies.nl/products/rw210/>, (visited 10.05.2017)

<sup>3</sup> Data sheet, <http://www.pacificrim.com.au/media/custom/upload/File-1367117101.pdf>, (visited 9.05.2017)

<sup>4</sup> [http://www.azurspace.com/images/0003429-01-01\\_DB\\_3G30C-Advanced.pdf](http://www.azurspace.com/images/0003429-01-01_DB_3G30C-Advanced.pdf), (visited 10.05.2017)

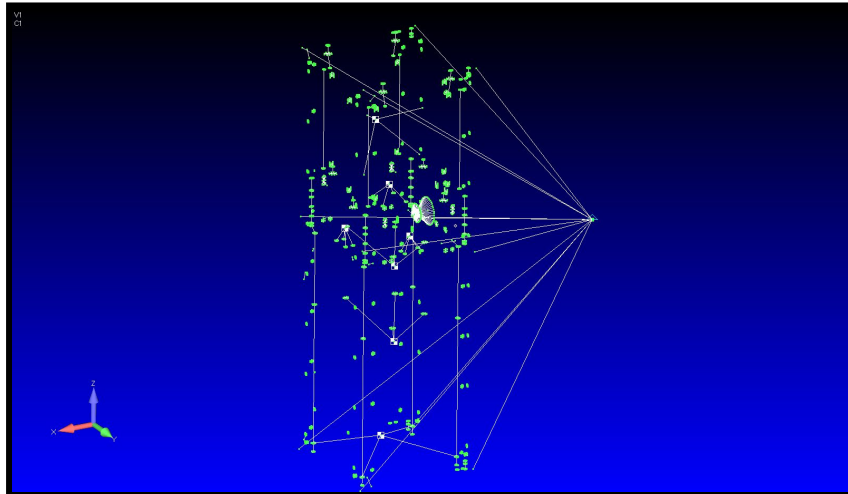


Figure 8b. Mass elements

#### 6.1.6. Mesh properties

The meshing properties were defined for the each shell element with detailed enough density and are shown in Figure 9. The meshing step between nodes is in the range of 1-3 mm. The current model has 61211 nodes, excluding those to be created for bolts and mass elements.

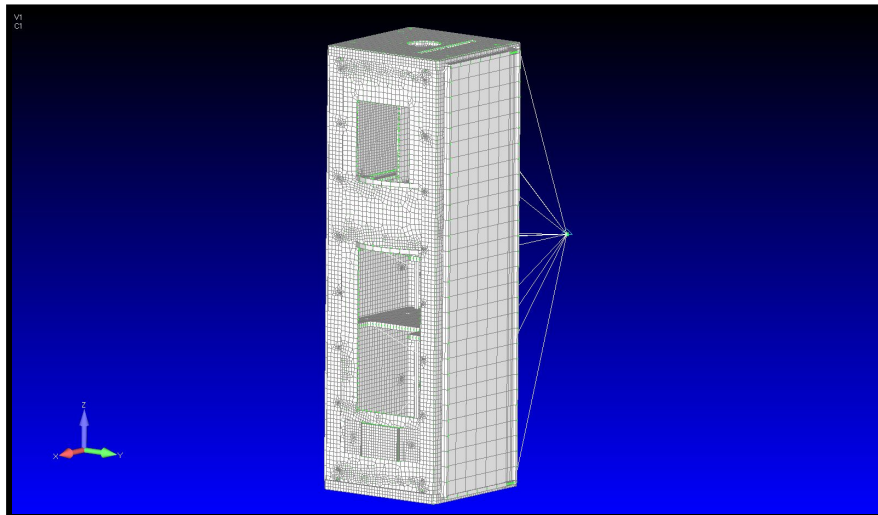


Figure 9. Mesh model

### 6.1.7. Boundary conditions

In this subsection constraints and loads are described.

#### 6.1.7.1. Constraints

In order to simulate an attachment of the satellite to the ISIPOD<sup>5</sup> deployer or to other relevant deployer, the rigid connections between the floating node and 12 points on the ESTCube's rails have been created. Eight points are located on the physical edges of the corners, meaning on Z-plus and Z-minus side panels and four points in the middle of U-frames.

In reality, the interface between the nanosatellite and deployer will have a rigid connection along the entire length of each rail. However, if such an approach is implemented into the simulation environment, the results might have more relaxed stresses and become more rigid than in the real conditions (private interview, Andrea Osti, SITAEL<sup>6</sup>).

#### 6.1.7.2. Loads

An overview of the loads requirements is given below.

- Resonance search

In this section natural frequencies and Q-factors for each mode are intended to be measured in simulation. They will be performed in conjunction with other vibration tests.

- High-level sine vibration

A high-level sinusoidal vibration test will be performed to ensure the article's ability to withstand constant acceleration over the whole band of interest. As per requirements in [Section 4](#), the high-level sine profile is shown in Table 2.

Table 2. High-level sine profile

Frequencies [Hz]	Level [g]
5	16
100	16

- Random vibration

A random vibration test is designed to study a more realistic vibration

<sup>5</sup> Data sheet, [https://www.isispace.nl/brochures/ISIS\\_ISIPOD\\_Brochure\\_v.7.11.pdf](https://www.isispace.nl/brochures/ISIS_ISIPOD_Brochure_v.7.11.pdf), (visited 10.05.2017)

<sup>6</sup> Company web page, <http://www.sitael.com/>, (visited 10.05.2017)

environment, when multiple subcomponents are excited at their natural frequencies. The test profile is shown in Table 3. The damping factor  $\zeta$  for the analysis is 2% as a starting value (private interview, Andrea Osti, SITAE) that might differ in reality and can be confirmed just after physical testing in the future.

Table 3. Random vibration test profile

Frequencies [Hz]	ASD [ $g^2/Hz$ ]
5	0.105
100	0.525
300	0.525
2000	0.023
Overall $g_{rms}$	17.38

## 6.2. Materials

The final materials selection will be made as an outcome of this analysis by negotiation with the manufacturing company. Initially, the aluminium alloy (AA) has been assigned for all metallic parts, for PCBs FR4, and for bolts Titanium Ti6Al4v grade 5. Hinges on deployable panels might be 3D metal printed from the AA or Ti, in the current model they are assigned as AA. Aluminium density properties are common (within a few percent) for 5000, 6000, and 7000 series. Based on the stresses occurred in the analysis the margins of safety for each material strengths will be calculated. Afterwards, the list of suitable materials will be created for each group of mechanical parts.

Table 4. Materials properties

Material	Density [ $kg/m^3$ ]	Poisson's ratio [-]	Modulus of elasticity [Gpa]	Ultimate tensile strength [MPa]	Tensile yield stress [MPa]
AA5083	2650	0.33	71	317	228
AA6062	2700	0.33	68.3	241	214
AA7075	2810	0.33	71.7	572	503
FR4	1500	0.118	240	70	65
Ti6Al4v	4500	0.34	114	1200	862

## 7. STRUCTURAL ANALYSIS RESULTS

### 7.1. Model check

The model check has to be performed in order to validate the structural analysis results that has been described in [Section 2.7](#). Before running the analysis the model is checked following instructions reported in [Appendix A](#) covering the consecutive points:

- Mass properties;
- Strain energy and stiffness max ratio check;
- Constraint check;
- Static load check;
- Free-free check.

#### 7.1.1. Mass properties

The mass distribution is obtained after performing the modal analysis; it is based on the mesh and materials properties and is shown in Table 5.

Table 5. FEA mass properties

Mass system	Axis mass [kg]	X-CoG	Y-CoG	Z-CoG
X	4.94	-1.17e-20	3.97e-02	-2.45e-04
Y	4.94	8.02e-02	1.05e-20	-2.44e-04
Z	4.94	8.026e-02	3.97e-02	1.22e-21

#### 7.1.2. Strain Energy and Stiffness Max Ratio Check

The total strain energy values and stiffness ratio has passed their limited values.

#### 7.1.3. Free-free check

The free-free check is passed. The analysis result with relaxed reference node shows that the first six natural frequencies are close to or equal to zero.

#### 7.1.4. Static load verification

The acceleration of  $9.81 \text{ m/s}^2$  has been applied separately to the each direction X, Y,

and Z. The evaluating constrain force in each direction has to be equal to the mass multiplied by the acceleration.

$$F = m \cdot a \quad (15)$$

$$F = 4.87 \text{ [kg]} \cdot 9.81 \text{ [m/s}^2\text{]} = 47.79 \text{ [N]}$$

Analysis results given by Femap are next:

- X direction:

*Maximum Value 2.48E-10. Output Vector 53 - T2 Constraint Force;*

*Minimum Value -47.79. Output Vector 52 - T1 Constraint Force.*

- Y direction:

*Maximum Value 1.81E-9. Output Vector 52 - T1 Constraint Force;*

*Minimum Value -47.79. Output Vector 53 - T2 Constraint Force.*

- Z direction:

*Maximum Value 5.09E-10. Output Vector 52 - T1 Constraint Force;*

*Minimum Value -47.79. Output Vector 54 - T3 Constraint Force.*

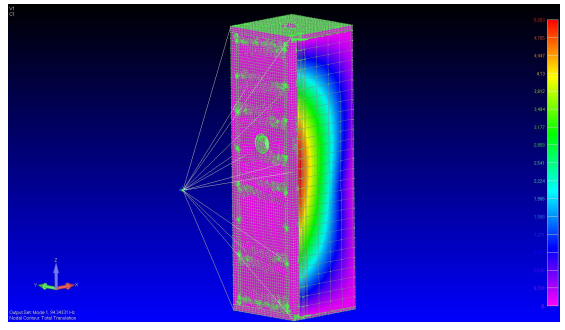
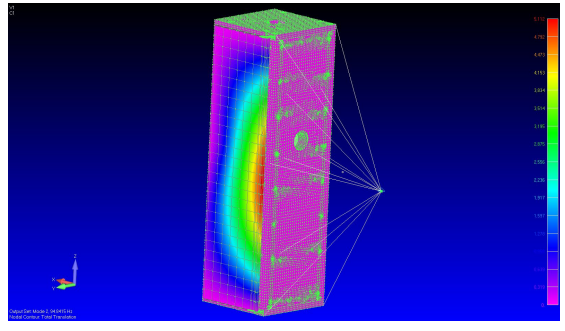
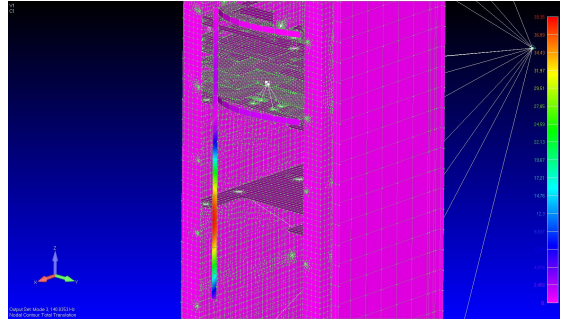
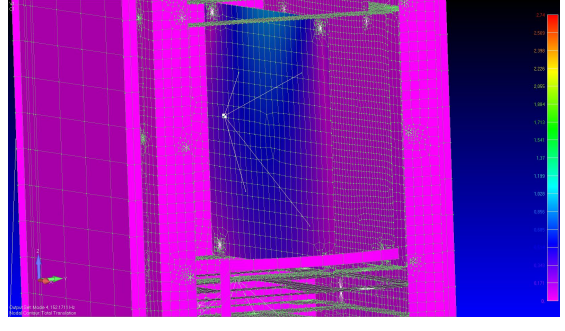
As is visible from the results, the values for X, Y, and Z translations (T1, T2, and T3 respectively) are satisfied. The negative numbers are obtained due to the applied force in the opposite direction with respect to the coordinating system.

## 7.2. Modal analysis

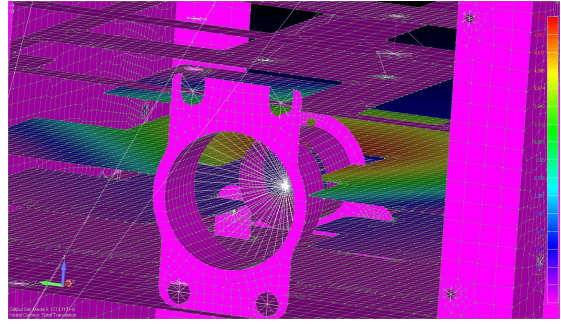
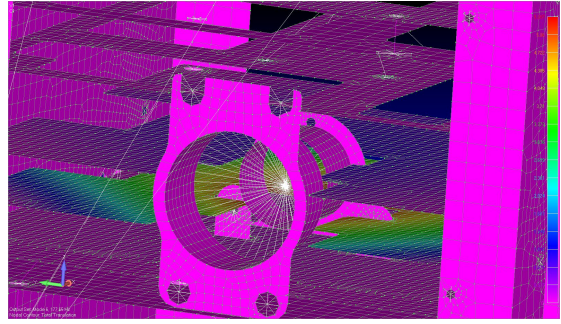
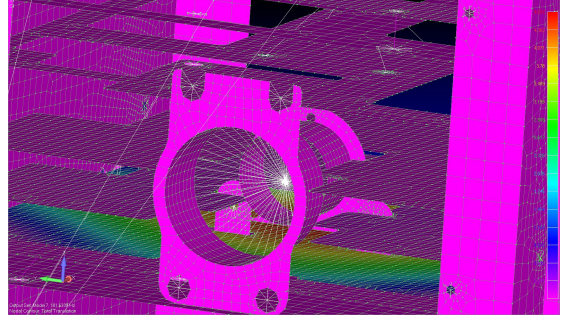
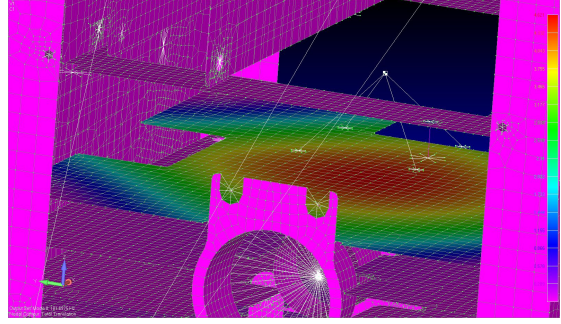
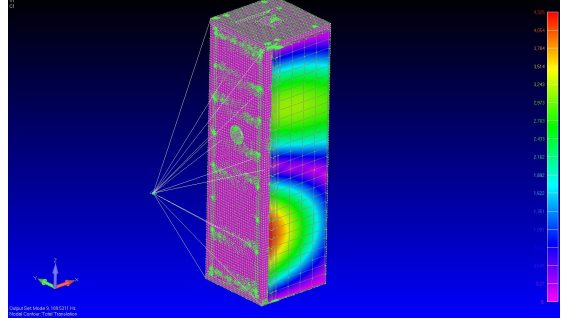
The modal analysis has been executed in order to determine the most predominant modes. It is done by evaluating the participation factor for each natural frequency. The participation factor is an indicator of modal mass that is presented for the translation and rotation in each direction, meaning six in total for each mode.

The first ten frequencies have been analysed for the current structure. Each mode is reported in Table 6 with the shell names, visual representations of the total translations, and frequencies at which it appears.

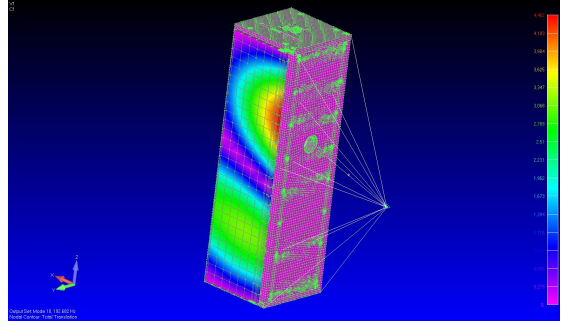
Table 6. Modal analysis results

Mode	Frequency, [Hz]	Shell	Visual representation of total translation
1	94.3	Y-minus deployable panel	
2	94.8	Y-plus deployable panel	
3	140.03	IFA	
4	152.1	Z-plus motor PCB	



5	177.17	Bus PCB B2	
6	177.65	Bus PCB B1	
7	181.6	Bus PCB B0	
8	181.7	Bus PCB B3	
9	189.5	Y-minus deployable panel	



10	192.6	Y-plus deployable panel	
----	-------	-------------------------------	--

For the participation factor, 300 modes have been examined in order to cover the range from the first mode up to 2000 Hz as shown in Figure 10. It is represented for translations in X, Y, and Z directions and rotations in X, Y, and Z directions.

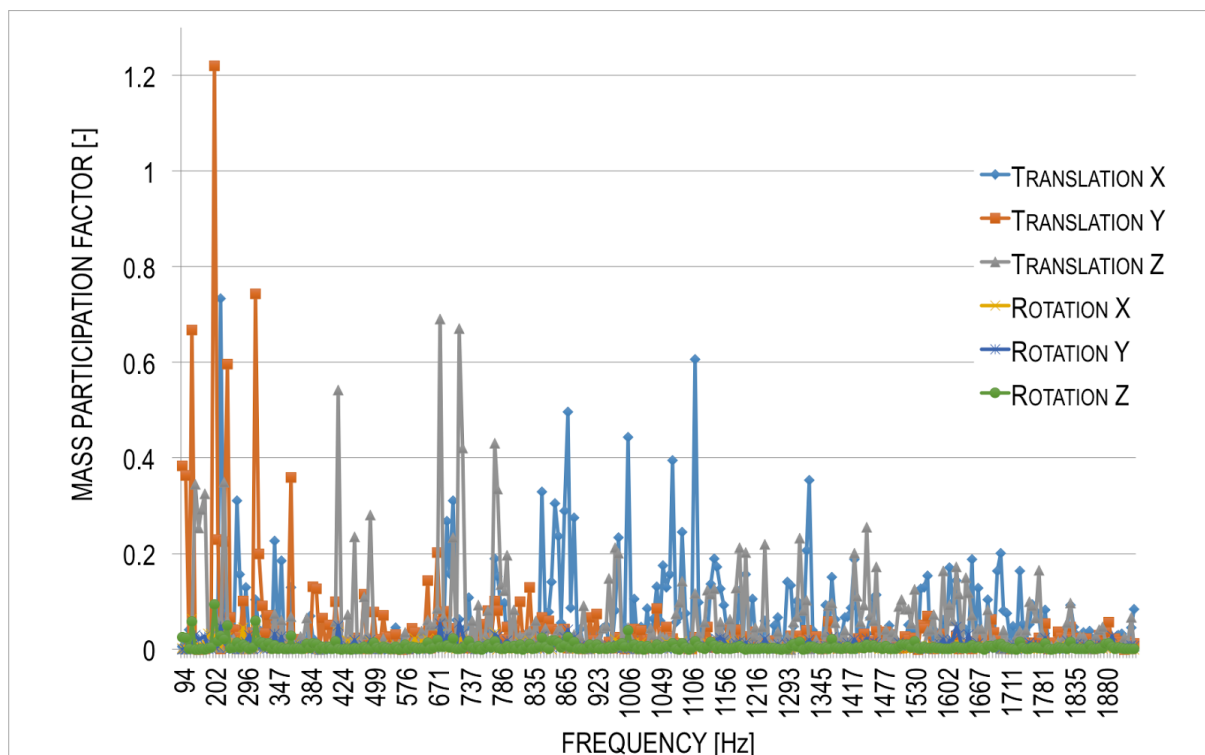


Figure 10. Participation factors for 300 modes

The big jump in translation in the Y direction with the participation mass factor over 1.2 (Figure 10) is caused by the polyether ether ketone (PEEK) matchbox. It is removed from the design and does not influence the general structure of the satellite.

### 7.3. High-level sine vibration

The high-level sine vibration analysis has been made for the entire structure described in [Section 6.1.3](#) in the each direction separately. The coordinate system for the analysis is the same as for the general satellite system presented in [Section 5](#). The high-level vibration profile is described in [Section 6.1.7.2](#). As outcome of analysis the three main values for each group of materials will be shown: displacements,

accelerations, and Von Mises stresses with one sigma confidence (three sigma confidence is implemented in the MoS calculations). The groups are formed depending on the materials and physical interface (e.g. bus main components); appropriate names are presented in Tables 7-9 for each direction.

### 7.3.1. High-level sine vibration in the X-direction

The highest occurred stresses in the X-direction for high-level sine vibration are for EO bottom plates, bus structure (bus bottom, top, and top-top plates), and U-frames. In addition, the IFA has high stress which was predictable considering thickness and size of the antenna. The stresses in tables have one sigma confidence. The conclusions for current section are presented in [Section 6.5.4](#).

The Von Mises stresses are visually represented in Figure 11 for the entire structure (left) and X-plus, X-minus side panels with bus (right).

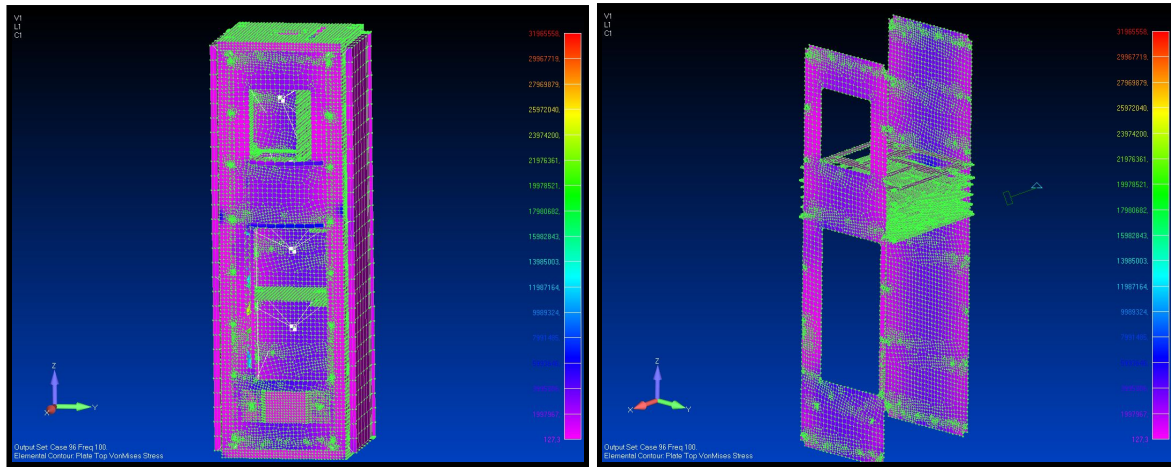


Figure 11. Von Mises stress for HS vibration in X direction

The grouped materials with results of analysis are presented in Table 7.

Table 7. High-level sine vibration in X direction results

Components	Displacement, $m$	Acceleration, $m/s^2$	Von Mises stress, $MPa$
<i>Aluminium group</i>			
Bus structure	6.42e-6	159.52	15.07
Star tracker structure	4.88e-6	158.88	3.32
EO bottom plate	9.05e-5	192.68	23.98
Z-plus PL structure	9.06e-6	160.53	7.811

Z-plus and Z-minus short side panels	1.14-6	157.41	6.91
Four long side panels	9.89e-5	196.01	8.68
Deployable panels	6.45e-6	159.51	2.88
Hinges	4.93e-6	158.90	5.47
U-frames	4.18e-6	158.61	14.17
<i>External group</i>			
IFA	6.30e-4	405.83	25.43
Coating experiment holder	5.98e-5	180.57	0.44
<i>FR4 group</i>			
Bus PCBs	3.46e-6	158.32	0.96
Z-plus payload PCBs	9.46e-6	160.69	11.66

Figure 12 shows graphs that represent relations between the frequency  $[Hz]$  and the acceleration  $[m/s^2]$  for two nodes. If one imagines the physical setup, it will look like two accelerometers – one attached to the attachment base and another on the side of the object which is the satellite in our case. This is a typical setup for physical testing, with two accelerometers better known as Control and Reference accelerometers. The graph shows comparison for reference node that simulates satellite attachment and Z-plus top cover plate (left) and X-minus side panel (right).

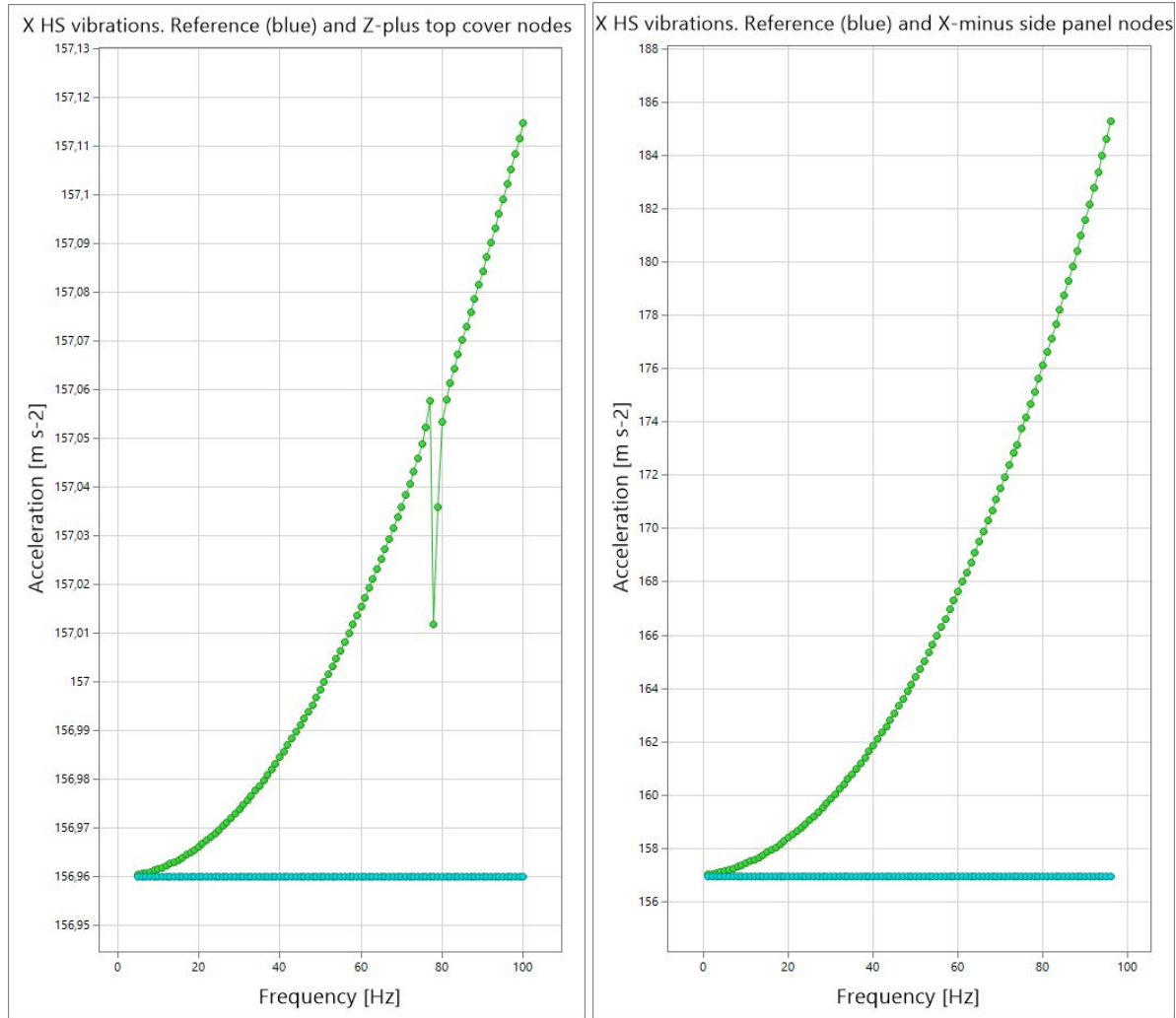


Figure 12. High-level sine vibration in X-direction. Acceleration graphs for various surfaces

### 7.3.2. High-level sine vibration in the Y-direction

The highest occurring stresses in the Y-direction for high-level sine vibration are for EO bottom plates and deployable panels (where the thinner large part is perpendicular to Y-axis). In addition, Z-plus payload PCBs have high stresses due to the perpendicular position to the Y-axis. The stresses in the tables have one sigma confidence. The conclusions for the current section are presented in [Section 6.5.4](#).

The Von Mises stresses are visually represented in Figure 13 for the entire structure (left) and EO bottom plate (right).

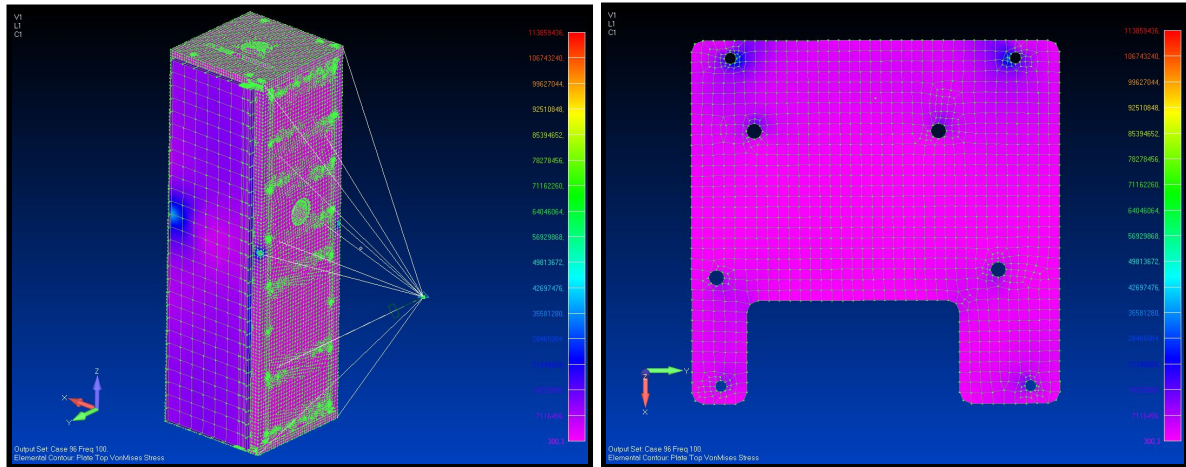


Figure 13. Von Mises stress for HS vibration in X direction

The grouped materials with results of analysis are presented in Table 8.

Table 8. HS vibration in Y direction results

Components	Displacement, $m$	Acceleration, $m/s^2$	Von Mises stress, $MPa$
<i>Aluminium group</i>			
Bus structure	8.47e-5	190.39	25.82
Star tracker structure	8.15e-5	189.13	14.39
EO bottom plate	1.87e-4	229.56	39.35
Z-plus PL structure	8.97e-5	192.35	19.89
Z-plus and Z-minus short side panels	3.58e-6	158.37	9.23
Four long side panels	1.24e-4	205.93	20.38
Deployable panels	1.23e-3	643.95	46.59
Hinges	1.22e-5	161.74	14.17
U-frames	1.03e-4	197.56	85.1
<i>External group</i>			

IFA	2.15e-5	165.44	2.35
Coating experiment holder	3.47e-6	158.33	0.37
<i>FR4 group</i>			
Bus PCBs	8.05e-5	188.71	1.94
Z-plus payload PCBs	4.87e-4	349.18	66.07

Figure 14 shows graphs that represent relations between the frequency [Hz] and the acceleration [ $m/s^2$ ] for two nodes. If one imagines the physical setup, it will look like two accelerometers – one attached to the attachment base and another on the side of the object which is the satellite in our case. This is typical setup for physical testing, with two accelerometers better known as Control and Reference ones. The graph shows comparison for reference node that simulates satellite attachment and Z-plus top cover plate (left) and Y-plus deployable panel (right).

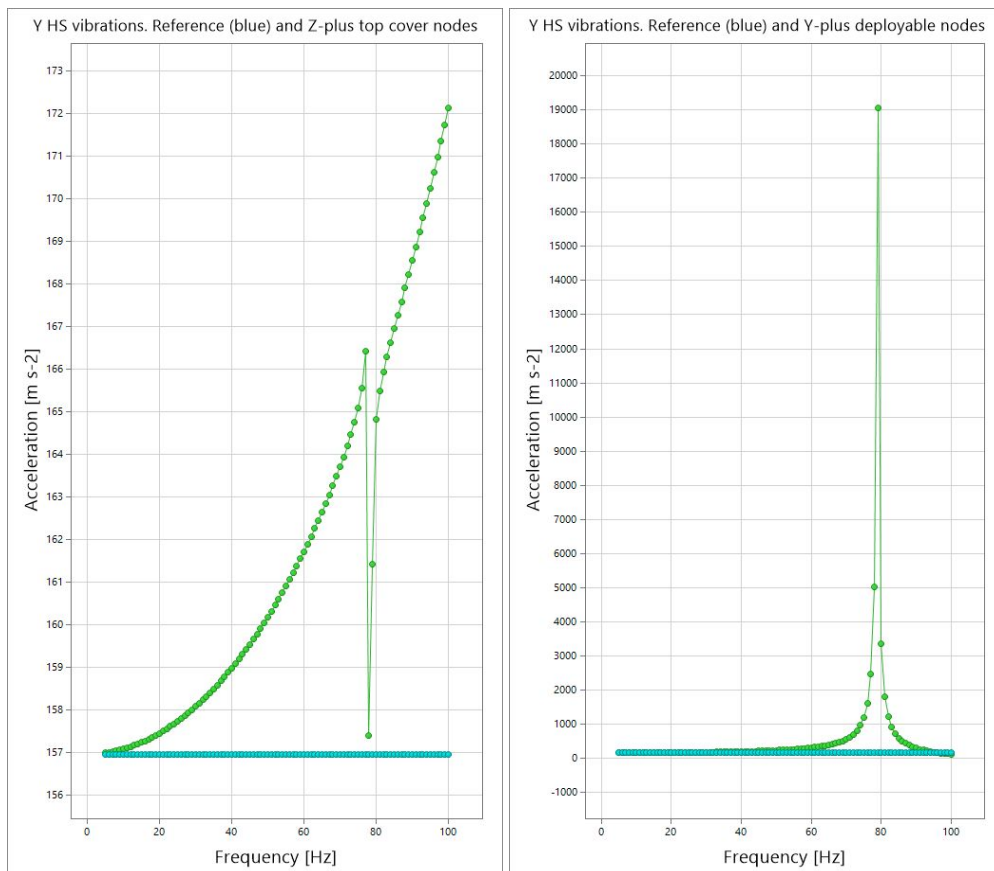


Figure 14. High-level sine vibration in Y-direction. Acceleration graphs for various surfaces

### 7.3.3. High-level sine vibration in the Z-direction

The highest occurred stresses in the Z-direction for high-level sine vibration are for EO bus structure (bus bottom, top, and top-top plates) and bus PCBs. The stresses in Table 10 have one sigma confidence. The conclusions for the current section are presented in [Section 6.5.4](#).

The Von Mises stresses are visually represented in Figure 15 for EO bottom plates and Z-minus short side panel (left) and bus structure with PCBs (right).

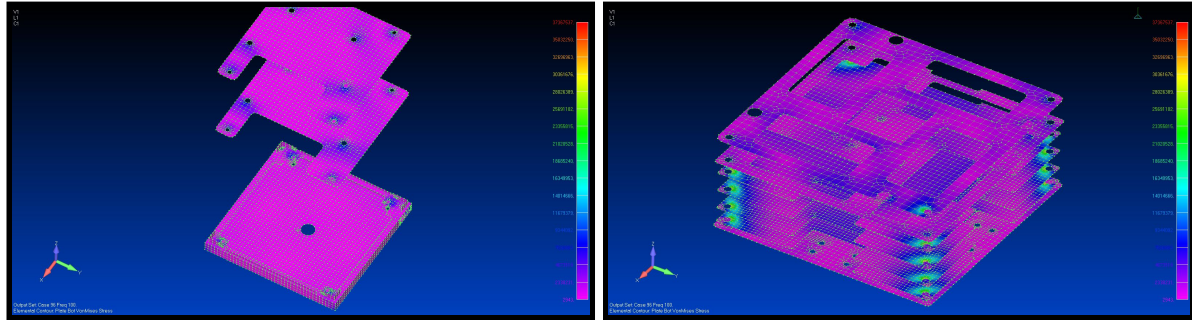


Figure 15. Von Mises stress for HS vibration in Z direction

The grouped materials with results of analysis are presented in Table 9.

Table 9. HS vibration in Z direction results

Components	Displacement, $m$	Acceleration, $m/s^2$	Von Mises stress, $MPa$
<i>Aluminium group</i>			
Bus structure	2.77e-5	167.89	25.36
Star tracker structure	8.63e-6	160.37	4.79
EO bottom plate	1.16e-5	161.55	11.86
Z-plus PL structure	3.28e-5	169.90	34.06
Z-plus and Z-minus short side panels	1.85e-5	164.26	12.02
Four long side panels	1.17e-6	157.42	3.41
Deployable panels	3.9e-6	158.50	1.78

Hinges	3.95e-6	158.52	7.32
U-frames	1.3e-6	157.47	6.48
<i>External group</i>			
IFA	6.5e-6	159.52	2.25
Coating experiment holder	1.59e-6	157.58	0.35
<i>FR4 group</i>			
Bus PCBs	2.89e-4	271.18	38.64
Z-plus payload PCBs	3.16e-5	169.43	12.81

Figure 16 shows graphs that represent relations between the frequency  $[Hz]$  and the acceleration  $[m/s^2]$  for two nodes. If one imagines the physical setup, it will look like two accelerometers – one attached to the attachment base and another on the side of the object which is the satellite in our case. This is typical setup for physical testing, with two accelerometers better known as Control and Reference accelerometers. The graph shows comparison for reference node that simulates satellite attachment and Z-plus top cover plate (left) and Y-plus deployable panel (right).



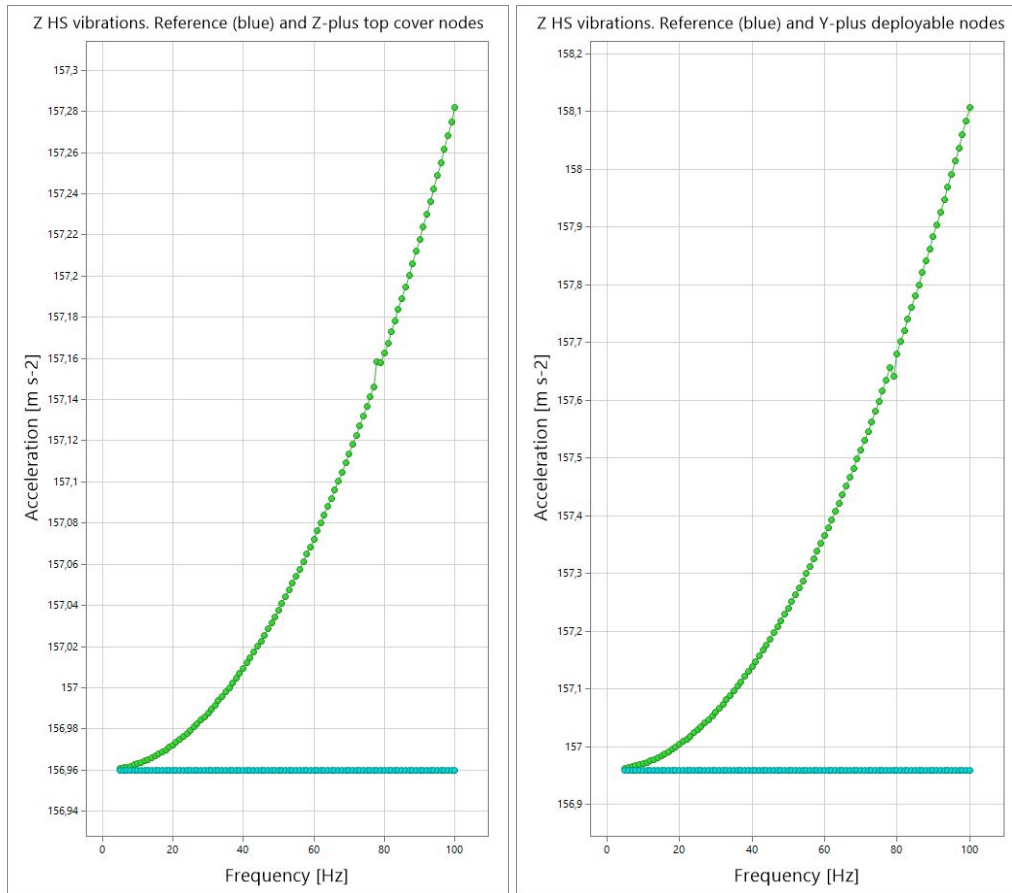


Figure 16. High-level sine vibration in Z-direction. Acceleration graphs for various surfaces

#### 7.3.4. High-level sine vibration conclusions

In this section the summary for high-level sine vibration is presented. The highest stress for each group has been implemented. For three sigma confidence the margin of safety (MoS) shown in Equation 14 will be calculated based on the strength of materials. For the aluminium group, three different series stated in [Section 6.2](#) will be implemented in order to widen the choice for the manufacturing process. The results of analysis are shown in Table 10 and 11, where green cells represent positive values of the MoS and red – negative. The stress analysis and their meaning are described in [Section 2.6](#).

Table 10. High-level stresses for aluminium group margin of safety

Component	Von Mises stress $1\sigma$ , [MPa]	Von Mises stress $3\sigma$ , [MPa]	Margin of Safety		
			AA5083	AA6062	AA7075
Bus structure	25.82	77.46	1.35	1.21	4.19

Star tracker structure	14.39	43.17	3.23	2.97	8.32
EO bottom plate	39.35	118.05	0.55	0.45	2.41
Z-plus PL structure	34.06	102.18	0.79	0.68	2.94
Z-plus and Z-minus short side panels	12.02	36.06	4.06	3.75	10.16
Four long side panels	20.38	61.14	1.98	1.80	5.58
Deployable panels	46.59	139.77	0.31	0.22	1.88
Hinges	14.17	42.51	3.29	3.03	8.47
U-frames	85.1	255.3	-0.29	-0.33	0.58
Coating experiment holder	0.44	1.32	137.50	128.99	304.54

The highest stress for U-frames is in the Y direction which is an order of magnitude higher than in other directions.

Table 11. High-level stresses for FR4 group margin of safety

Component	Von Mises stress $1\sigma$ , [MPa]	Von Mises stress $3\sigma$ , [MPa]	Margin of Safety
Bus PCBs	38.64	115.92	-0.55
Z-plus payload PCBs	66.07	198.21	-0.74

The highest stress for bus PCBs is in the Z direction, for Z-plus payload PCBs in Y-direction. **Negative values mean that indicated components did not satisfy stress analysis, it does not mean that the components will fail, though there is a probability of such an event to occur.**

## 7.4. Random vibration

The random vibration analysis has been done for the entire structure described in [Section 2](#) in the each direction separately. The coordinate system for the analysis is the same as for the general satellite system. The random profile PSD function is described in [Section 6.1.7.2](#). As outcome of analysis the three main values for each group of materials will be shown: displacements, accelerations, and Von Mises stresses with one sigma confidence (three sigma confidence is implemented in the MoS calculations presented in [Section 7.4.4](#)). The groups are formed depending on the materials and physical interface (e.g. bus main components); appropriate names are presented in Tables 12-14 for each direction.

### 7.4.1. Random vibration in the X-direction

The highest occurred stresses in the X-direction for random vibration are for EO bottom plates, and Z-plus payload structure. In addition, the IFA has high stress which was predictable considering thickness and size of antenna. The stresses in Table 12 have one sigma confidence. The conclusions for current section are presented in [Section 6.5.4](#).

The Von Mises stresses are visually represented in Figures 17a, 17b, and 17c for the entire structure, U-frame, and EO bottom plate respectively.

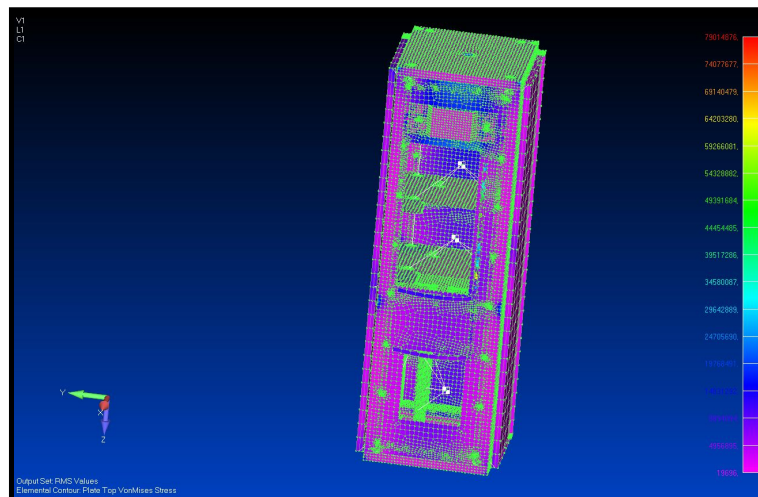


Figure 17a. Von Mises stress for random vibration in X direction for the entire satellite

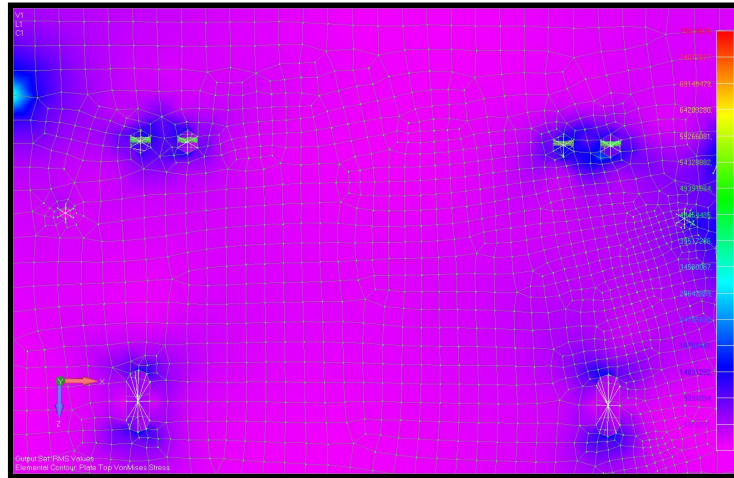


Figure 17b. Von Mises stress for random vibration in X direction for the Y-plus U-frame on the bus attachment side

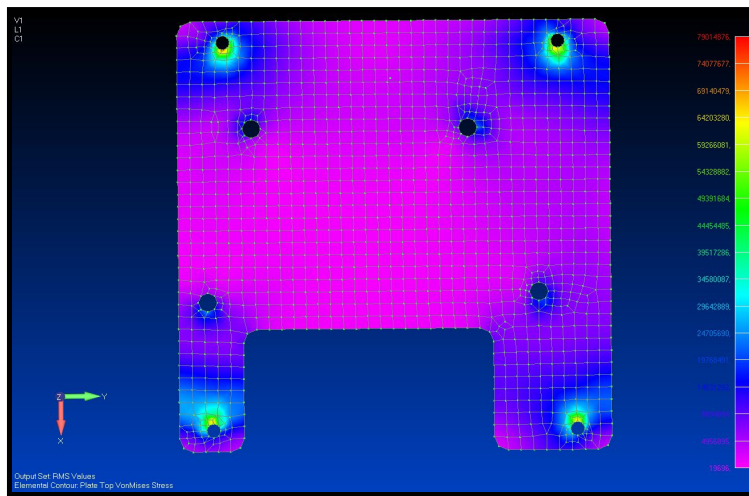


Figure 17c. Von Mises stress for random vibration in X direction for the EO bottom plate

The grouped materials with results of analysis are presented in Table 12.

Table 12. Random vibration in X direction results

Components	Displacement, $m$	Acceleration, $m/s^2$	Von Mises stress $1\sigma$ , $MPa$
<i>Aluminium group</i>			
Bus structure	2.02e-6	200.27	48.41
Star tracker structure	1.47e-6	173.93	9.6
EO bottom plate	8.9e-5	823.49	79.61

Z-plus PL structure	2.91e-6	221.22	54.58
Z-plus and Z-minus short side panels	3.4e-7	171.1	34.93
Four long side panels	1.47e-4	1617.65	49.31
Deployable panels	2.23e-6	219.58	15.16
Hinges	1.93e-6	204.75	32.61
U-frames	1.37e-6	184.58	38.49
<i>External group</i>			
IFA	7.75e-4	1071.27	55.25
Coating experiment holder	6.52e-5	757.54	2.34
<i>FR4 group</i>			
Bus PCBs	1.04e-6	175.54	11.44
Z-plus payload PCBs	3.05e-6	228.37	31.88

Figures 18a and 18b show graphs that represent relations between the frequency  $[Hz]$  and the acceleration  $[m/s^2]$  for two nodes. If one will imagine the physical setup, it will look like two accelerometers – one attached to the attachment base and another on the side of the object which is the satellite in our case. This is a typical setup for physical testing, with two accelerometers better known as Control and Reference accelerometers. The graph shows a comparison between a reference node that simulates satellite attachment and four different surfaces specified in Figures 18a and 18b.

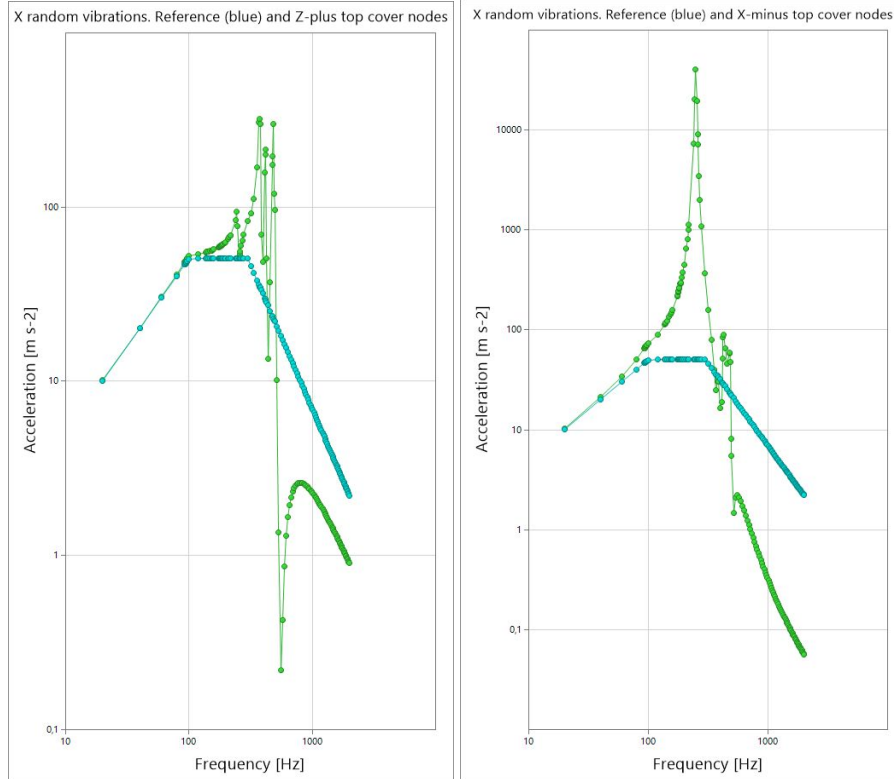


Figure 18a. Random vibration accelerations in logarithmic scale in X-direction.  
Acceleration graphs for various surfaces

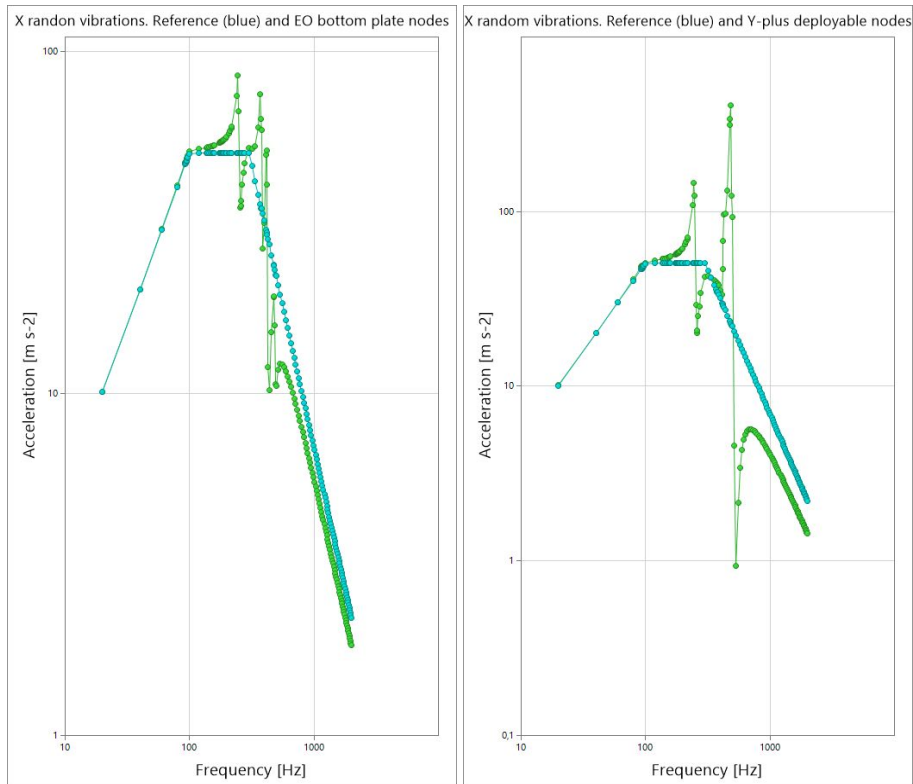


Figure 18b. Random vibration accelerations in logarithmic scale in X-direction.  
Acceleration graphs for various surfaces

### 7.4.2. Random vibration in the Y-direction

The highest occurred stresses in the Y-direction for random vibration are for U-frames, EO bottom plates, and Z-plus payload PCBs. The stresses in Table 13 have one sigma confidence. The conclusions for the current section are presented in [Section 6.5.4](#).

The Von Mises stresses are visually represented in Figures 19a, 19b, 19c and 19d for the entire structure, U-frame, EO bottom plate, and Z-plus payload motor PCB respectively.

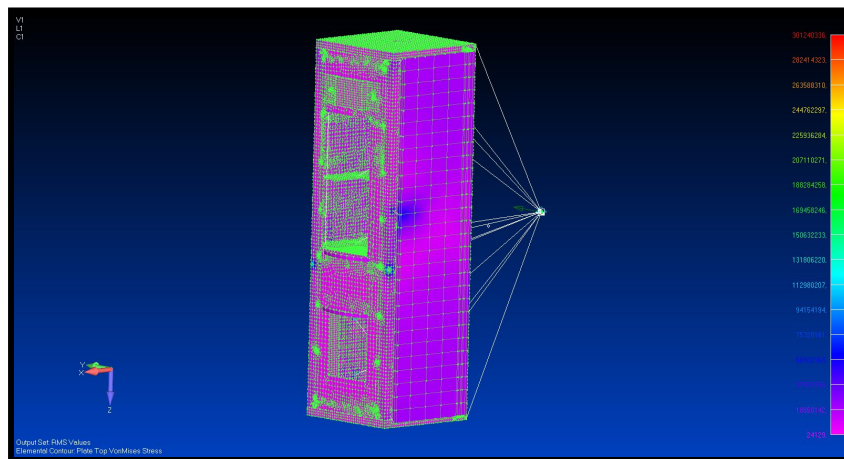


Figure 19a. Von Mises stress for random vibration in Y direction for the entire satellite

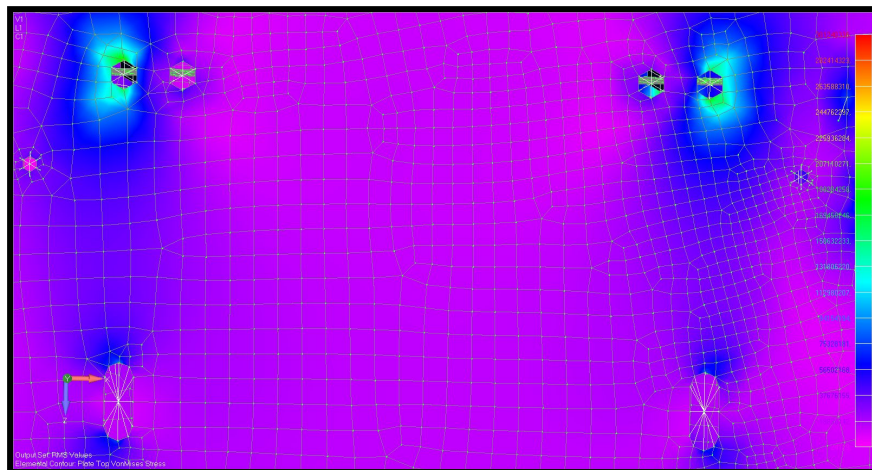


Figure 19b. Von Mises stress for random vibration in Y direction for the Y-plus U-frame on the bus attachment side



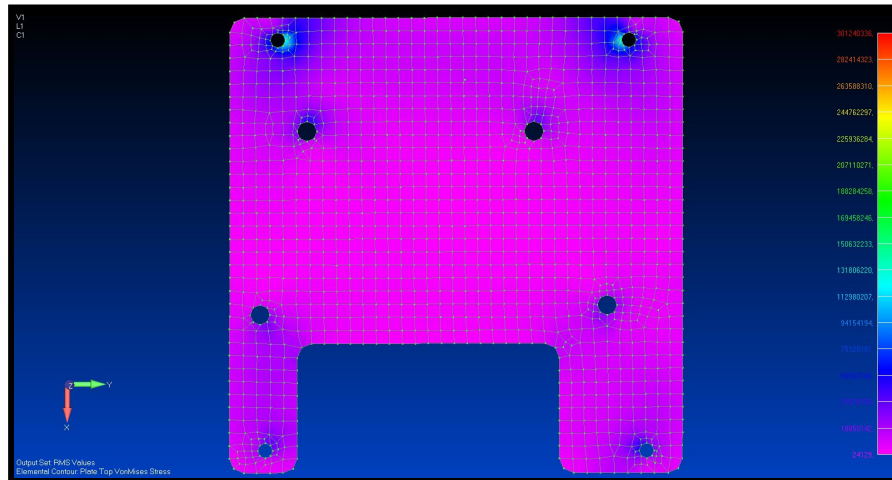


Figure 19c. Von Mises stress for random vibration in Y direction for the EO bottom plate

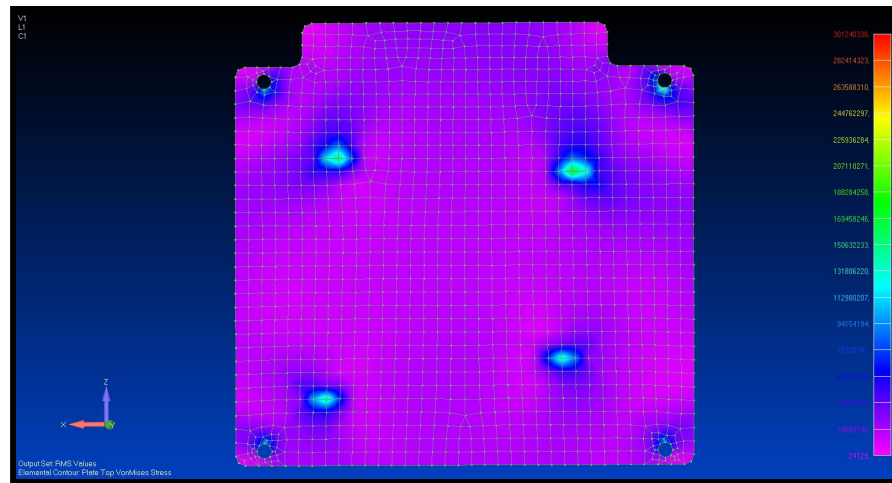


Figure 19d. Von Mises stress for random vibration in Y direction for the Z-plus payload motor PCB

The grouped materials with results of analysis are presented in Table 13.

Table 13. Random vibration in Y direction results

Components	Displacement, $m$	Acceleration, $m/s^2$	Von Mises stress, $MPa$
<i>Aluminium group</i>			
Bus structure	4.56e-5	401.99	65.45
Star tracker structure	4.64e-5	406.29	41.26



EO bottom plate	2.6e-4	1144.38	141.49
Z-plus PL structure	4.43e-5	410.72	47.27
Z-plus and Z-minus short side panels	8e-7	170.49	56.05
Four long side panels	2.12e-4	1140.31	47.15
Deployable panels	2.15e-3	1666.25	68.54
Hinges	4.6e-7	199.9	32.94
U-frames	6.36e-5	499.64	209.17
<i>External group</i>			
IFA	1.6e-5	405.96	9.99
Coating experiment holder	9.6e-7	171.337	1.70
<i>FR4 group</i>			
Bus PCBs	4.55e-5	400.277	17.85
Z-plus payload PCBs <sup>7</sup>	6.72e-4	1122.01	147.38

Figures 20a and 20b show graphs that represent relations between the frequency [Hz] and the acceleration [ $m/s^2$ ] for two nodes. If one will imagine the physical setup, it will look like two accelerometers – one attached to the attachment base and another on the side of the object which is the satellite in our case. This is typical setup for physical testing, with two accelerometers better known as Control and Reference accelerometers. The graph shows a comparison between a reference node that simulates satellite attachment and four different surfaces specified in Figures 18a and 18b.

<sup>7</sup> The highest stress is concentrated on the motor PCB

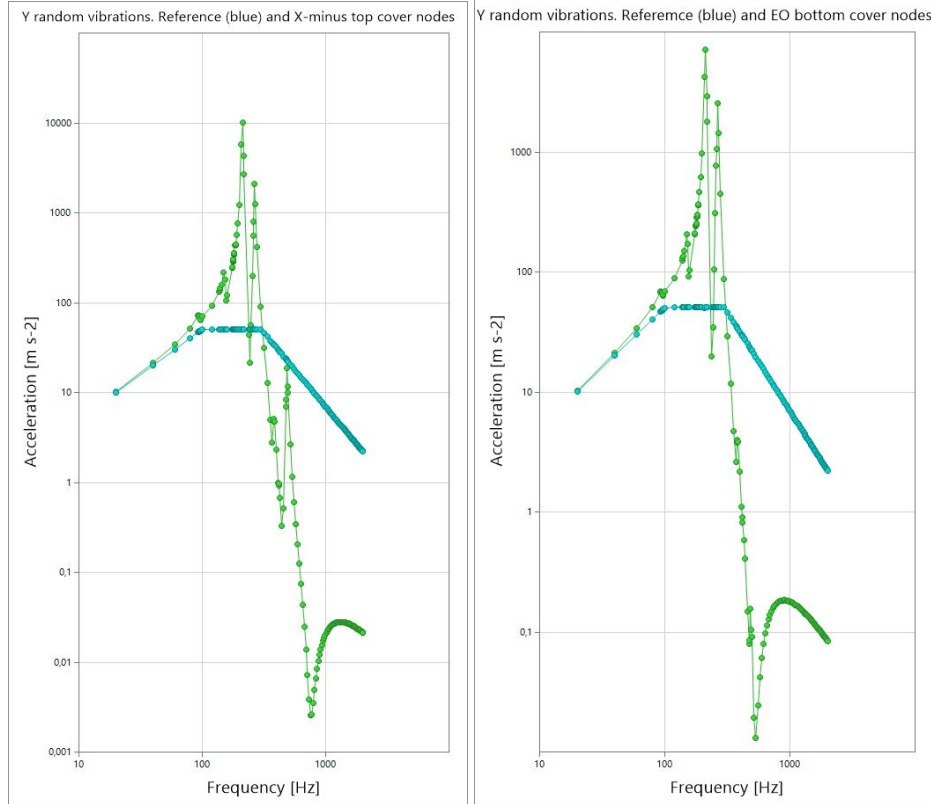


Figure 20a. Random vibration accelerations in logarithmic scale in Y-direction.  
Acceleration graphs for various surfaces

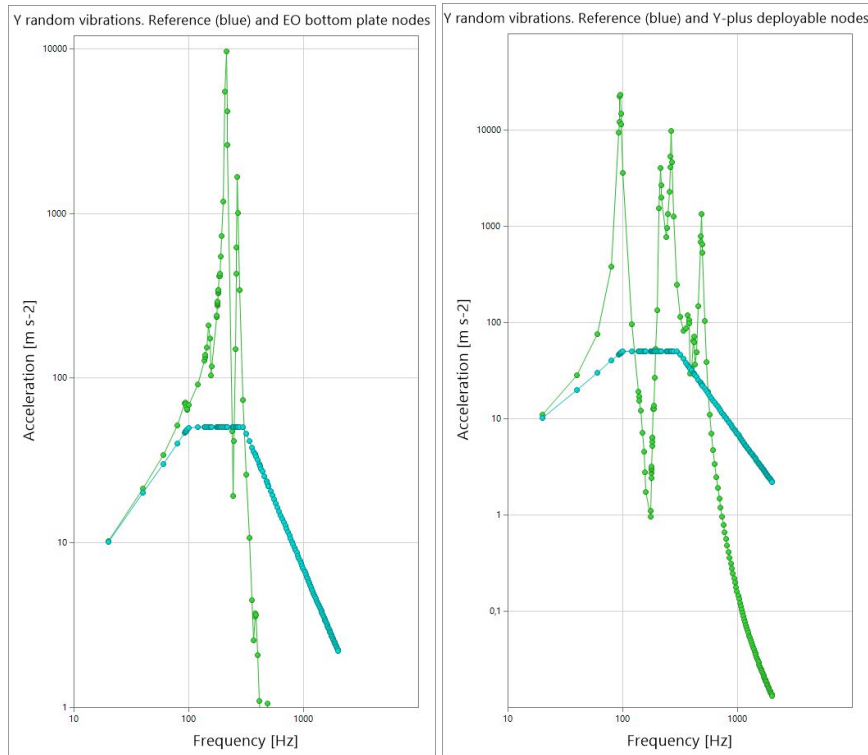


Figure 20b Random vibration accelerations in logarithmic scale in Y-direction.  
Acceleration graphs for various surfaces

### 7.4.3. Random vibration in the Z-direction

The highest occurred stresses in the Y-direction for random vibration are for Z-plus payload structure, bus structure, and bus PCBs. The stresses in Table 14 have one sigma confidence. The conclusions for the current section are presented in [Section 6.5.4](#).

The Von Mises stresses are visually represented in Figures 21a, 21b, and 21c for the entire structure, U-frame, and EO bottom plate respectively.

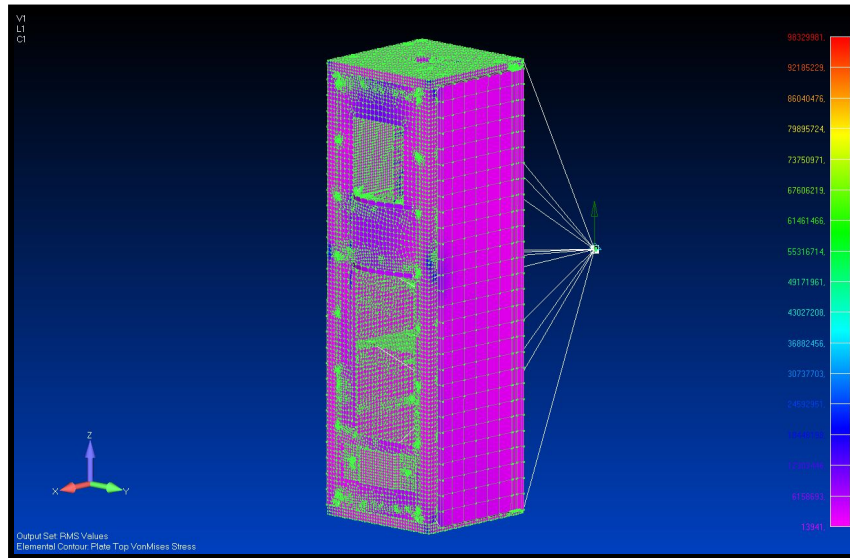


Figure 21a. Von Mises stress for random vibration in Z direction for the entire satellite

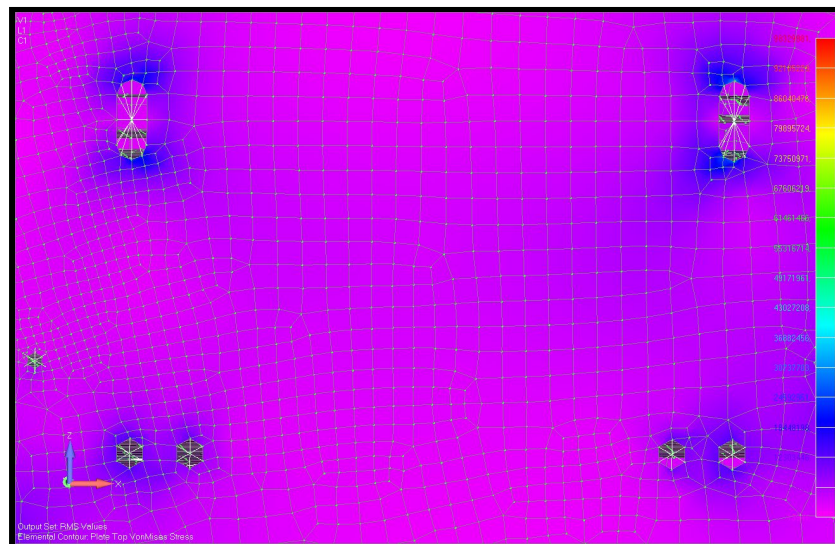


Figure 21b. Von Mises stress for random vibration in Z direction for the Y-plus U-frame on the bus attachment side

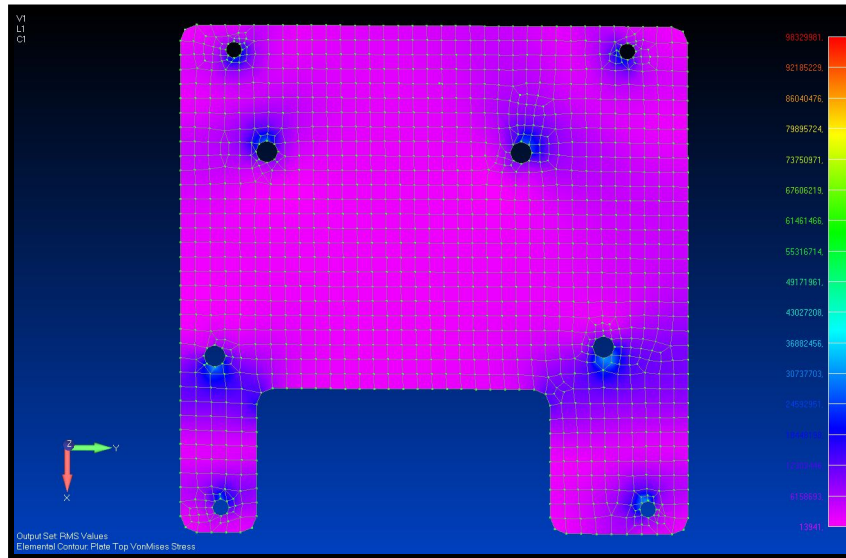


Figure 21c. Von Mises stress for random vibration in Z direction for the EO bottom plate

The grouped materials with results of analysis are presented in Table 14.

Table 14. Random vibration in Z direction results

Components	Displacement, $m$	Acceleration, $m/s^2$	Von Mises stress, $MPa$
<i>Aluminium group</i>			
Bus structure	1.24e-5	558.38	81.81
Star tracker structure	3.04e-6	231.07	14.58
EO bottom plate	4.26e-6	278.25	40.64
Z-plus PL structure	1.59e-5	648.33	105.22
Z-plus and Z-minus short side panels	7.75e-6	403.28	36.89
Four long side panels	3.3e-7	170.46	36.95
Deployable panels	1.29e-6	185.64	15.96
Hinges	1.37e-6	183.73	30.03
U-frames	3.7e-7	170.61	42.07

<i>External group</i>			
IFA	4.09e-6	427.82	18.45
Coating experiment holder	4.7e-7	171.93	1.94
<i>FR4 group</i>			
Bus PCBs	4.03e-4	1047.29	101.38
Z-plus payload PCBs <sup>8</sup>	1.48e-5	617.71	54.76

Since the stress for the bus PCBs has been very high, the stress distribution has been shown additionally in Figure 21d. Such distribution applies for each PCB in the bus.

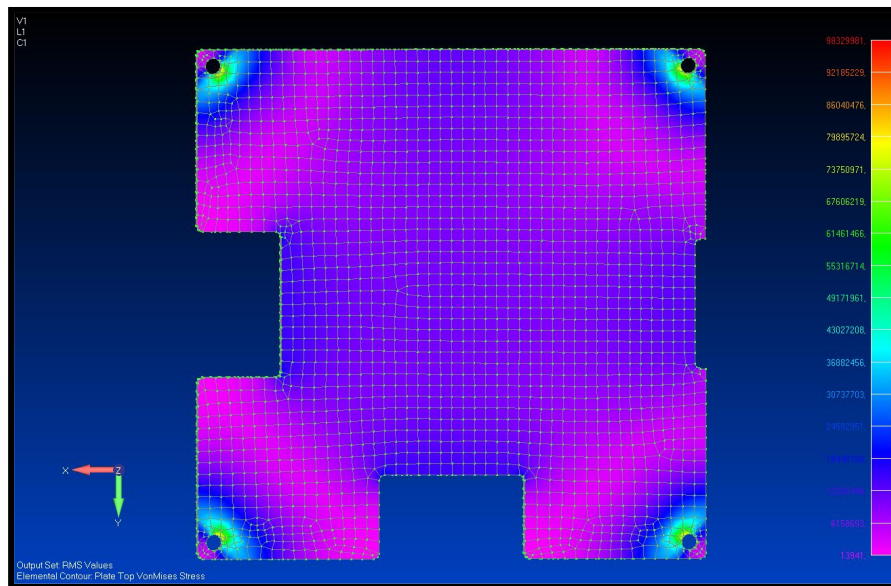


Figure 21d. Von Mises stress for random vibration in Z direction for the bus PCB

Figures 22a and 22b show graphs that represent relations between the frequency [Hz] and the acceleration [ $m/s^2$ ] for two nodes. If one will imagine the physical setup, it will look like two accelerometers – one attached to the attachment base and another on the side of the object which is the satellite in our case. This is typical setup for physical testing, with two accelerometers better known as Control and Reference accelerometers. The graph shows a comparison between a reference node that simulates satellite attachment and four different surfaces specified in Figure 22a and 22b.

<sup>8</sup> The highest concentration of stress on the motor PCB due to the reel movement in the Z direction.

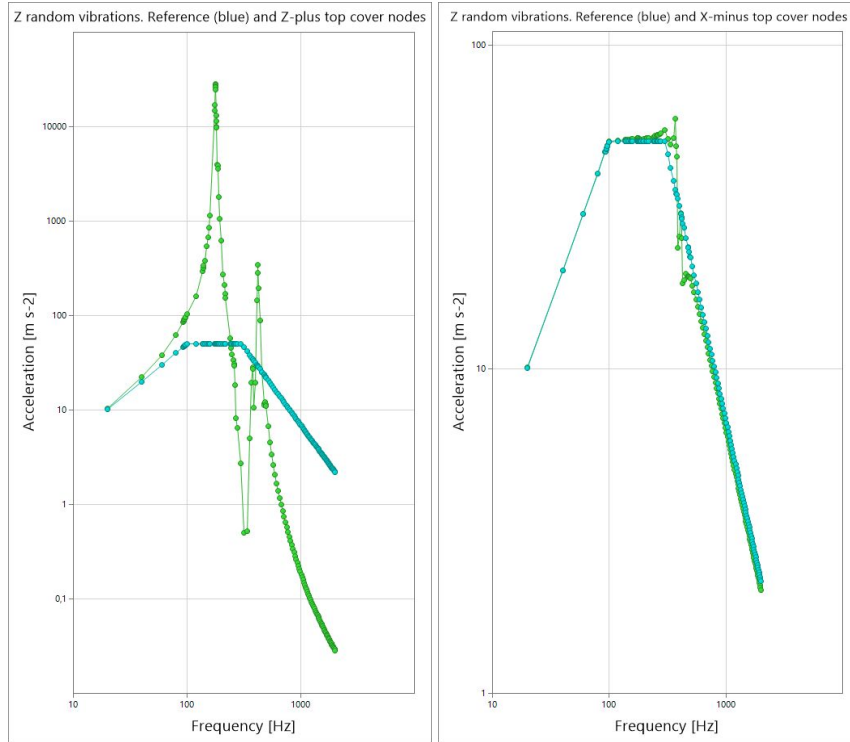


Figure 22a. Random vibration accelerations in logarithmic scale in Z-direction.  
Acceleration graphs for various surfaces

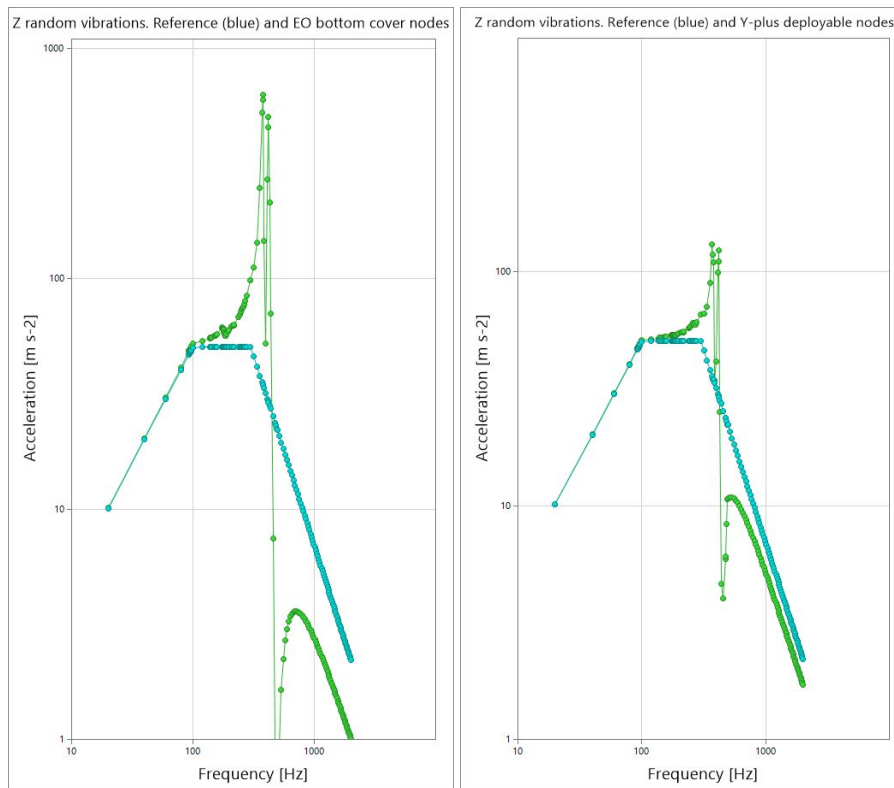


Figure 22a. Random vibration accelerations in logarithmic scale in Z-direction.  
Acceleration graphs for various surfaces

#### 7.4.4. Random vibration analysis conclusions

In this section the summary for random vibration is presented. The highest stress for each group will be implemented. For three sigma confidence the margin of safety (MoS) shown in Equation 14 will be calculated based on the strength of materials. For aluminium group three different series stated in [Section 6.2](#) will be implemented in order to wider the choice for manufacturing process. The results of analysis are shown in Table 15 and 16, where green cells represent positive values of the MoS and red – negative. The stress analysis and their meaning are described in [Section 2.6](#).

Table 15. Random stresses for aluminium group margin of safety

Component	Von Mises stress $1\sigma$ , [MPa]	Von Mises stress $3\sigma$ , [MPa]	Margin of Safety		
			AA5083	AA6062	AA7075
Bus structure	81.81	245.43	-0.26	-0.30	0.64
Star tracker structure	41.26	123.78	0.47	0.38	2.25
EO bottom plate	141.49	424.47	-0.57	-0.60	-0.05
Z-plus PL structure	105.22	315.66	-0.42	-0.46	0.27
Z-plus and Z-minus side panels	56.05	168.15	0.08	0.02	1.39
Four long side panels	49.31	147.93	0.23	0.16	1.72
Deployable panels	68.54	205.62	-0.11	-0.17	0.96
Hinges	32.94	98.82	0.85	0.73	3.07
U-frames	209.17	627.51	-0.71	-0.73	-0.36
Coating experiment holder	2.34	7.02	24.98	23.39	56.32

The highest stress for U-frames and EO bottom plates is in the Y direction which is an order of magnitude higher than in other directions. The Z-plus PL structure has the highest stress in the Z direction.

Table 16. Random stresses for FR4 group margin of safety

Component	Von Mises stress $1\sigma$ , [MPa]	Von Mises stress $3\sigma$ , [MPa]	Margin of Safety
Bus PCBs	101.38	304.14	-0.83
Z-plus payload PCBs	147.38	442.14	-0.88

The highest appeared stress for bus PCBs is in Z direction, for Z-plus payload PCBs in Y-direction. **Negative values mean that indicated components did not satisfy stress analysis. It does not mean that components will fail, though there is a probability of such event to occur.**



## 8. CONCLUSIONS

This thesis presents a structural analysis of the ESTCube-2 nanosatellite and gives an overview on the structural design and main design drivers. The main aim of this thesis was to simulate vibration and loads during launching of the spacecraft.

The satellite has been modeled using SolidWorks software and analysed in FEMAP with Nastran simulation environment. The ESTCube-2 model experienced simplifications as some components have been simulated as the mass elements described in [Section 6.1.5](#).

Particularly, the high-level sine and random vibrations have been treated as per the worst case scenario in the analysis. The margins of safety (MoS) have been calculated for each group of materials based on the Von Mises stresses for different aluminium series (5000, 6000, and 7000). The densities of materials are common but strengths are significantly different. Moreover, the manufacturing process for some aluminium series is more complex than for others.

The results for high-level sine vibration stresses in the structure are presented in [Section 7.3.4](#); the results for random vibration stresses are presented in [Section 7.4.4](#). Some parts made from specific materials have negative values of margin of safety, which means they did not pass the stress analysis. It does not mean that the components will fail, though there is a probability of such an event to occur. Two solutions can be implemented for components that have failed stress analysis: the first is taking the risk without redesigning or improving the part and relying on physical testing; the second is to allocate the budget in terms of time and resources for redesigning the structural part.

Considering this particular case, the vibration profile for structural simulation most likely will be less harmful, also time and resources in terms of engineers are limited. The damping factor is somewhat uncertain before physical testing and has been discussed in [Section 6.1.7.2](#). Moreover, the satellite attachment had 12 points on the rails for simulations, where in reality the structure will be in full attachment along each rail, making the attachment more robust. Aforementioned statements in this paragraph have a valuable influence on the structural stresses results, thus some improvements for each component will be implemented instead of full satellite redesign, as the results are conservative at this point. Future work is described in [Section 8.1](#). In addition, in order to make a quality analysis, the loads have to be predicted. However, knowledge of nanosatellite load environments is limited as nanosatellites are typically launched as a secondary payloads [25].

## **8.1 Future work**

Structural improvements will cover increased thickness in areas where applicable, involving thicker spacers, especially for PCB and the camera's bottom plate in order to increase contact area, as well as some supporting structures. The negotiation with manufacturer (ProtoLab, Estonia) will be executed based on the design solution, chosen materials, and components manufacturing process. Afterwards, the manufactured hardware will be physically tested on the vibration bench (one and three axes accelerometers). The results will be a subject of comparison with structural simulation in order to understand and improve structural simulations in the future.

## **ACKNOWLEDGMENTS**

This thesis would not have been possible unless the hard work of the ESTCube team from the beginning until now. I am deeply grateful to every ESTCuber, particularly to Andris Slavinskis, Erik Ilbis, Hendrik Ehrpais, Henri Kuuste, Indrek Sünter, Tõnis Eenmäe and finnish e-sailors – Pekka, Petri, and Jouni. The experience of being in the team turned thesis writing into rather relatively simple task than a huge pain in asini. I want to thank Tartu Observatory for the facility and support, and Archimedes Foundation for the travel allowance in order to visit International Astronautical Congress and ESA's conference on space debris. I received a generous support from University of Tartu and Estonian Foreign Ministry's Development Cooperation and Humanitarian Aid funds that supported my studies. I have greatly benefit from an internship in SITael (former AlmaSpace) that gave a basic and unique knowledge on the structural analysis; I want to thank my internship supervisor Andrea Osti who gave advices during thesis work. My heartfelt appreciation goes to Wolf Geppert who organized spectacular schools around the globe on the astrobiological subjects and brought a huge inspiration and outstanding academic fellows together. I want to thank Photon Engineering for providing the license for the FRED software employed for the baffle stray light analysis. Many thanks to Nina Kopacz for her excellent editing skills and fun times in general. In process of writing this thesis I met one special person – Mari Mäna, whom I am especially thankful for her support and warm hugs. Moreover, many thanks to all charming people I have met on my way in Estonia, especially in the Tolstoi house – Angela (special thank for the critical editing of this thesis), Meri, Marie Bastian, Gretta, Romane, Julien, Kaisa, Maari, Mats, Kristine, Judith...I would continue this list, but unfortunately the thesis has limitation on the page number. Finally, I would like to express my very profound gratitude to my parents (Ivan and Tanya) and sister Diana, even despite the fact that they do not have any idea what is my thesis about. As the last word, I would like to thank Mark Wahlberg for his tune "Good Vibrations".

## REFERENCES

- [1] Origin of the Sputnik project,  
[http://www.russianspaceweb.com/sputnik\\_origin.html](http://www.russianspaceweb.com/sputnik_origin.html), (visited 14.03.2017)
- [2] Elizabeth Howell, Sputnik: The Space Race's Opening Shot, 2012,  
<http://www.space.com/17563-sputnik.html>, (accessed August 7, 2016)
- [3] Nanosatellite database by Erik, Figures: CubeSat type.  
<http://www.nanosats.eu/index.html#figures>. (accessed 8.04.2017)
- [4] ISIPOD CubeSat deployer, ISIS,  
[https://www.isispace.nl/brochures/ISIS\\_ISIPOD\\_Brochure\\_v.7.11.pdf](https://www.isispace.nl/brochures/ISIS_ISIPOD_Brochure_v.7.11.pdf), (last visited 9.04.2017)
- [5] KickSat, product description, <http://kicksat.github.io> , (last visited 9.04.2017)
- [6] ESTCube-1. The course of mission, <https://www.estcube.eu/en/estcube-1>, (last visited 10.04.2017)
- [7] Thomas P. Sarafin (editor), *Spacecraft structures and mechanisms: From Concept to Launch*, Microcosm, Inc., Kluwer Academic Publishers, 1995
- [8] S. W. Samwel, Low Earth Orbit Atomic Oxygen Erosion Effect on Spacecraft Materials, *Space Research Journal*, ISSN 1819-3382, 2013
- [9] Barter, Neville J., ed. 1982. *TRW space Data*. S&TG Marketing communication. Redondo Beach, CA: TRW, Inc.
- [10] Ryan Simmons, et. al., Miles' equation, poster at FEMSI workshop 2001: Innovative FEM Solutions to Challenging Problems, NASA Goddard Space Flight Center, May 2001
- [11] Hurty, W.C. and M.F. Rubinstein. 1964. *Dynamics of structures*. Englewood Cliffs, NJ: Prentice-Hall, Inc.
- [12] Jones, R. 1975. An approximate expression for the fundamental frequency of vibration of elastic plates. *Journal of Sound and Vibrations*. 38(4): 503-504
- [13] P. Janhunnen, Electric sail for spacecraft propulsion, *J. Propul. Power*, 20 (4) (2004) 763–764
- [14] Janhunnen, P., Electrostatic plasma brake for deorbiting a satellite, *J. Prop. Power*, 26, 370–372, 2010

- [15] Iakubivskiy I., Ehrpais H., et.al., ESTCube-2 mission analysis: plasma brake experiment for deorbiting, Proceedings of the 67th International Astronautical Congress, 2016
- [16] Andris Slavinskis, et.al, High spin rate magnetic controller for nanosatellite, 2014, Acta Astronautica 95, p.218-226
- [17] ESA Space Debris Mitigation Handbook, Release 1 on April 7, 1997 and updated in July 2002 (Ref: QINETIQ/KI/SPACE/CR021539, ESA Contract 14471/00/D/HK)
- [18] Iakubivskiy I., Ehrpais H., et.al., ESTCube-2 plasma brake payload for effective deorbiting, Proceedings of the 7th European Conference on Space Debris, ESA/ESOC, 2017
- [19] The ECSS-E-30 Mechanical Engineering. Standard. M. Klein. Mechanical Engineering Department, ESA Directorate for Technical and Operational Support, ESTEC, Noordwijk, The Netherlands, 2001
- [20] Products: 3U CubeSat structure, Innovative Solutions in Space, <https://www.isispace.nl/product/3-unit-cubesat-structure/>, (accessed 27.04.2017)
- [21] Slavinskis Andris, et.al, ESTCube-1 in-orbit experience and lessons learned. Aerospace and Electronic Systems Magazine, IEEE (Volume: 30, Iss.:8, 12-22) 10.1109/MAES.2015.150034
- [22] CubeSat design specification. Rev.9, p.4, [http://org.ntnu.no/studsat/docs/proposal\\_1/A8%20-%20Cubesat%20Design%20Specification.pdf](http://org.ntnu.no/studsat/docs/proposal_1/A8%20-%20Cubesat%20Design%20Specification.pdf) (accessed 27.04.2017)
- [23] Hendrik Ehrpais, et.al, Nanosatellite spin-up using magnetic actuators: ESTCube-1 flight results, Acta Astronautica 128 (2016), 210-216
- [24] Sünter I., Kuuste H., Iakubivskiy I., et.al., DUAL-CAMERA PAYLOAD for ESEO, Proceedings of the 4S Symposium, 2016
- [25] Spaceflight, Inc. (2013), Secondary Payload Users Guide, SF-2100-PUG-00001, Rev D 2013-03-05

## **Non-exclusive licence to reproduce thesis**

I, Iaroslav Iakubivskyi,

1. Herewith grant the University of Tartu a free permit (non-exclusive licence) to reproduce, for the purpose of preservation, including for the purpose of preservation in the DSpace digital archives until expiry of the term of validity of the copyright “Nanosatellite Anatomy Analysis: The Second Generation of ESTCube”, supervised by Andris Slavinskis and Erik Ilbis.
2. Making the thesis available to the public is not allowed.
3. I am aware of the fact that the author retains the right referred to in point 1.
4. This is to certify that granting the non-exclusive licence does not infringe the intellectual property rights or rights arising from the Personal Data Protection Act.

Tartu, 15.05.2017

## Appendix A Mechanical mathematical model requirements

The following checks shall be performed on the finite element model (FEM) prior to be used and delivered in the FEMAP software simulations.

### 1. Mass Distribution Check

Success criteria are the following:

- Mass distribution shall be in good accordance with the unit mass distribution;
- Mass figure shall be the same for the three axes X, Y and Z;
- Figures on the diagonal of the center of gravity (CoG) mass matrix must be zero.

### 2. Strain Energy and Stiffness Max Ratio Check

Strain energy and stiffness max ratio check shall be performed to evaluate if the FEM is well conditioned from mathematical standpoint.

This check is made running the FEM with NASTRAN SOL 103 using the SUPPORT card.

The strain energy is calculated for every SUPPORT point and written in the ".f06" file also the MAXRATIO figure is written in the ".f06" file.

Success criteria are the following:

- The value of the strain energy must be limited to  $5e - 3 J$ ;
- The maximum ratio represents the ratio between the higher and the lower value of the stiffness matrix. The maximum allowed value for the MAXRATIO is  $1e7$ .

### 3. Constraint Check

The purpose of the constraint check is to verify if unintended grounding are present.

This check is made running the FEM, in the free-free condition, with NASTRAN SOL 103 analysis and with GROUNDCHECK command.

The results of this check are given in the ".f06" file. The system automatically executes checks.

### 4. Static Load Check

The purpose of the static load check is to confirm that total forces at the interface of the model divided by the acceleration must be equal to the unit/model mass.

Success criteria are the following:

- The total force computed at the interface shall be equal to the unit mass multiplied by the acceleration;
- No constraint forces should occur at points other than legitimate boundary condition locations.

### 5. Free-Free Check

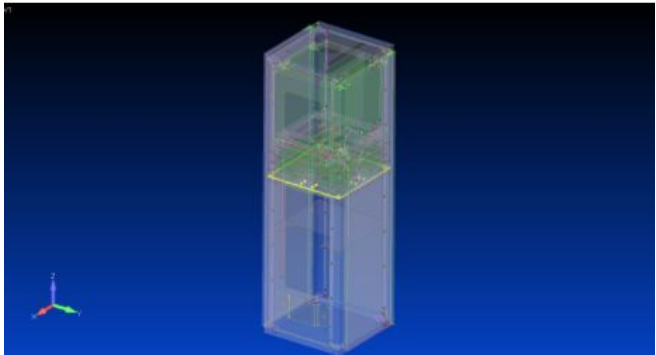
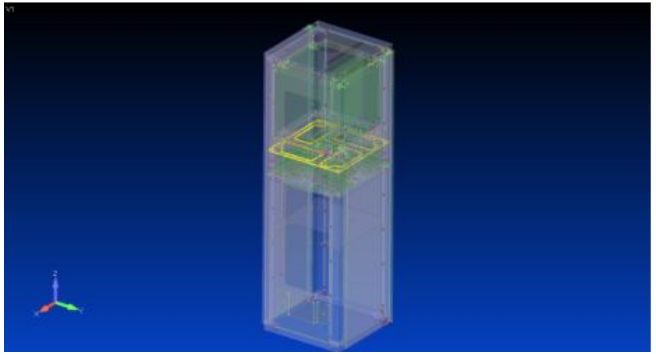
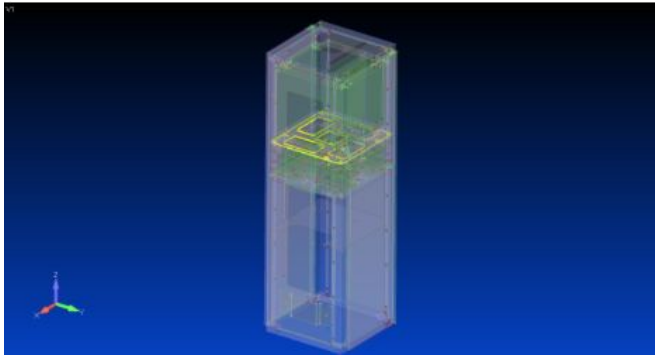
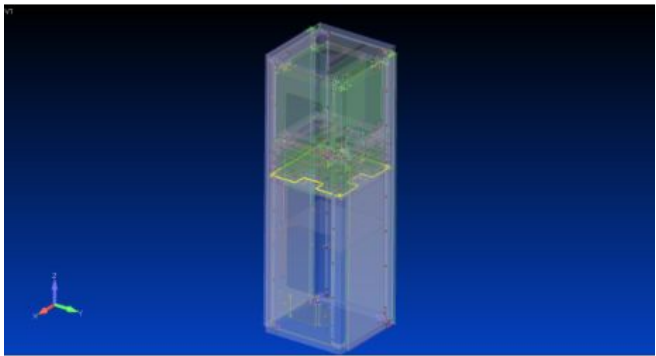
The purpose of the Free-Free check is to verify the rigid body modes of the model.

Success criteria are the following:

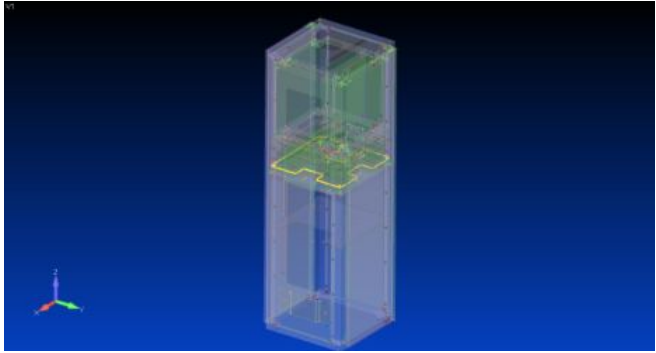
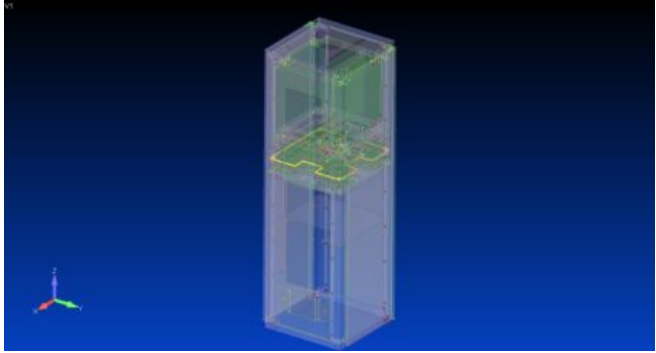
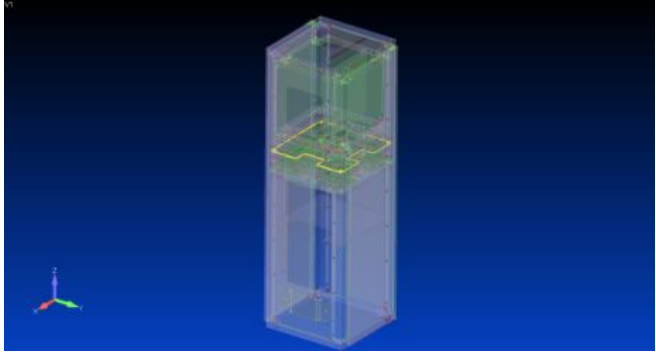
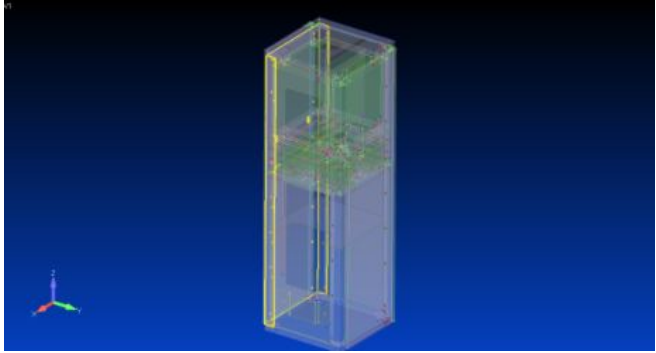
- The computed frequencies of first six modes shall be lower than  $1e - 3 Hz$ .

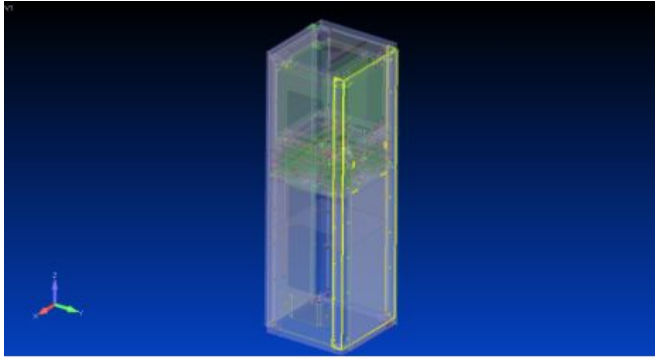
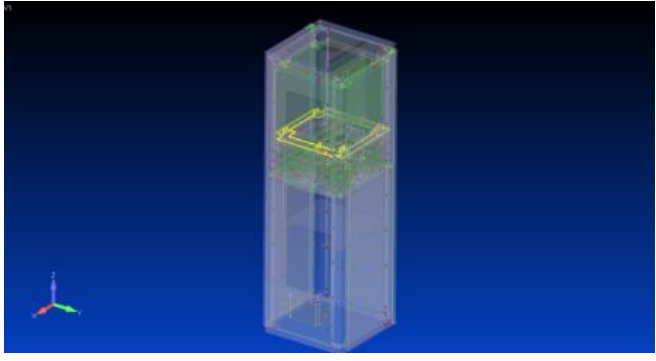
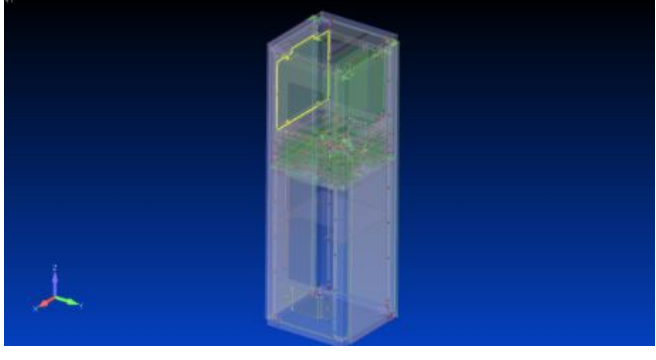
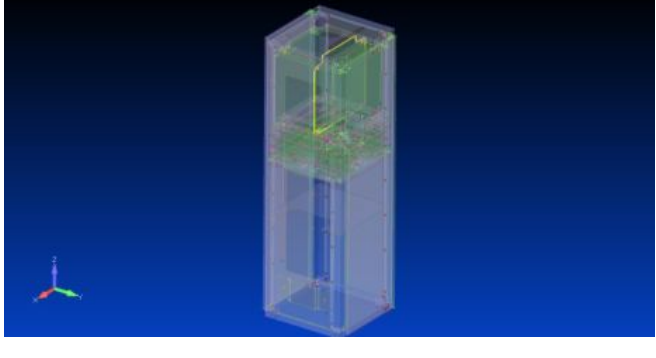
## Appendix B FEA model description

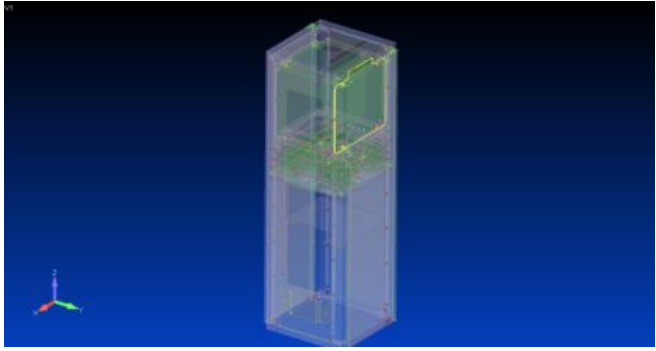
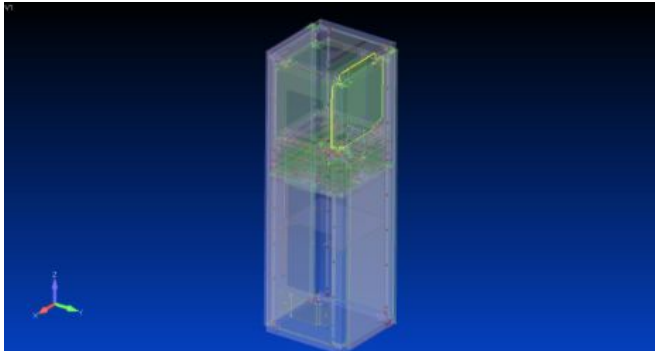
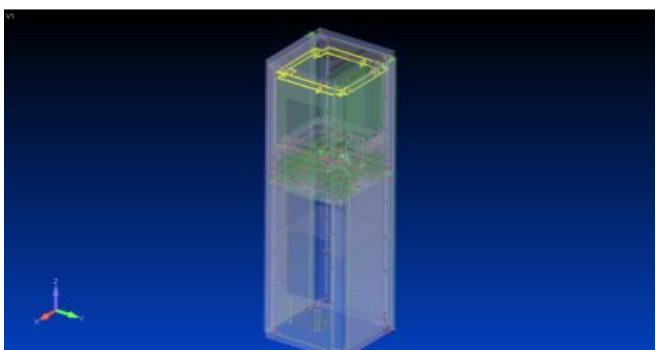
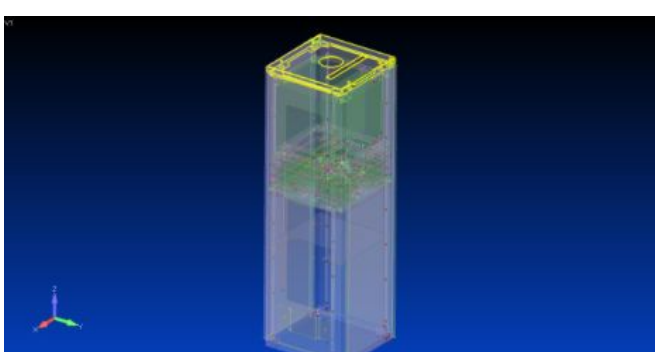
The table in the current Appendix represents model description as the shell elements in the FEMAP software.

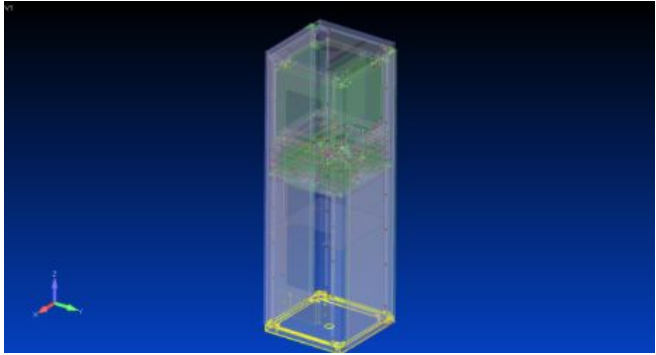
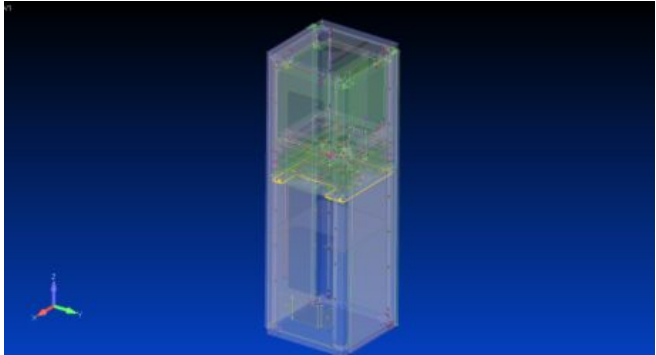
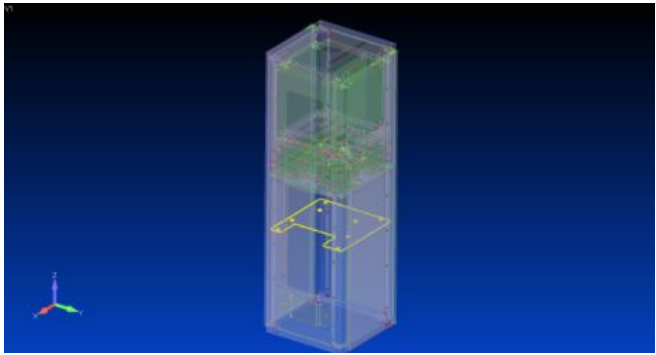
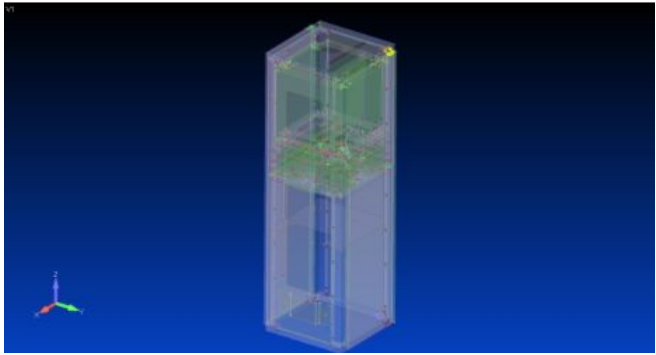
Shell element	Thickness, [mm]	Visual representation
Bus bottom plate	4	
Bus top plate	4	
Bus top-top plate	2.5	
Bus PCB B0	1.6	

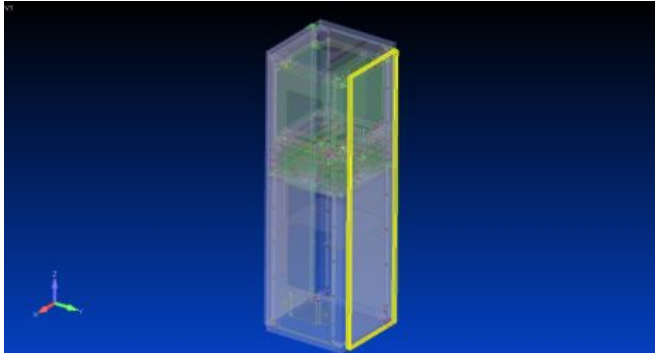
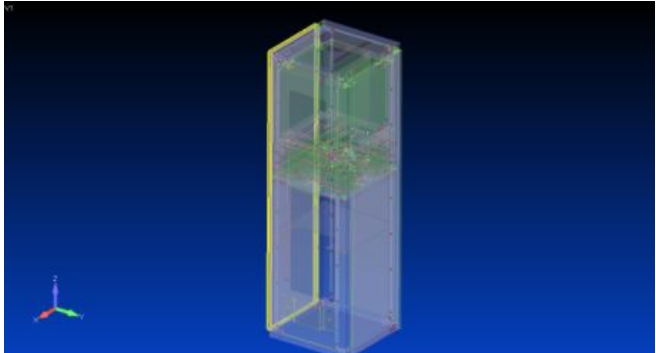
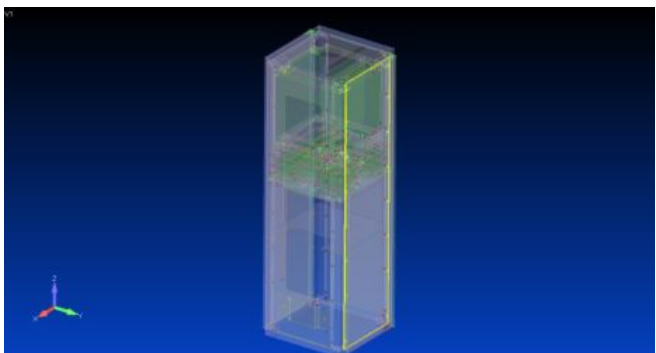
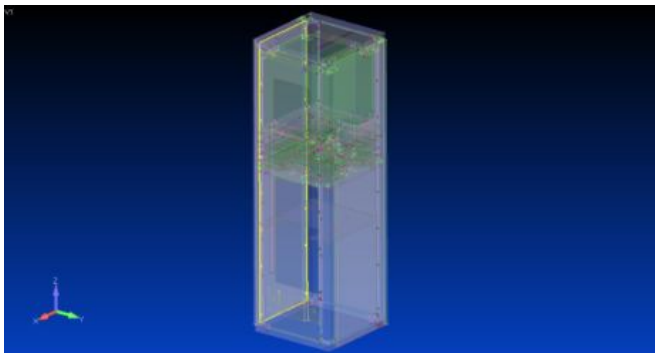


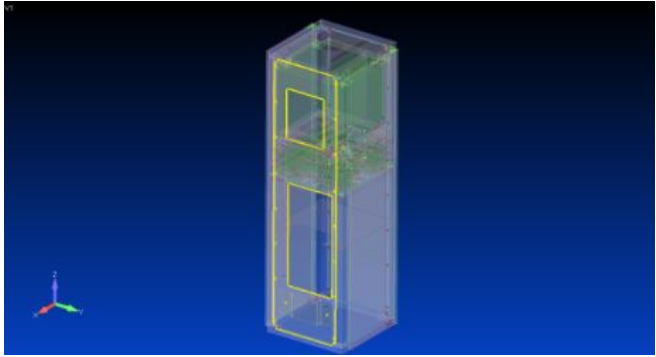
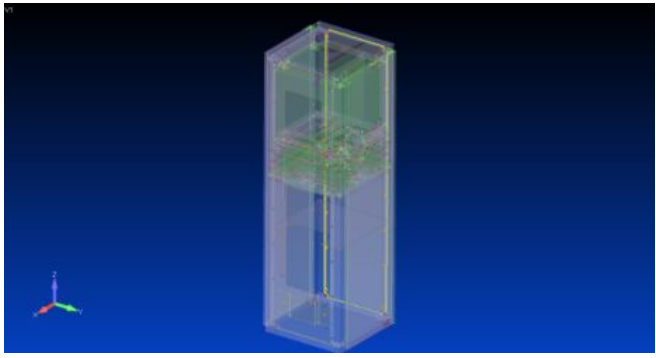
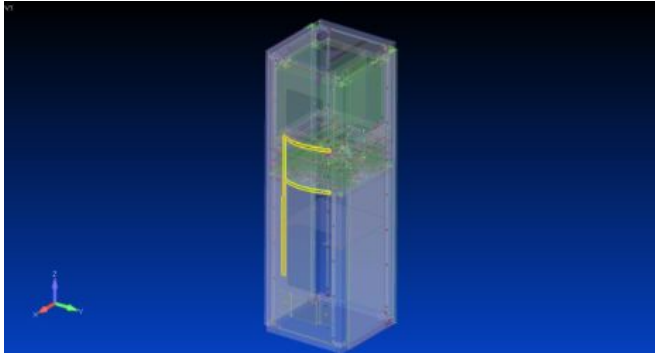
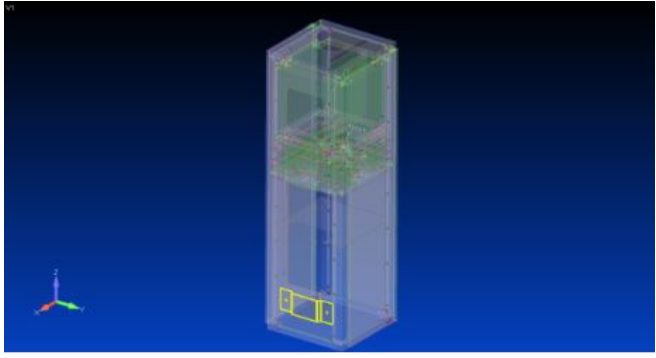
Bus PCB B1	1.6	
Bus PCB B2	1.6	
Bus PCB B3	1.6	
U-frame Y-minus	2.2	

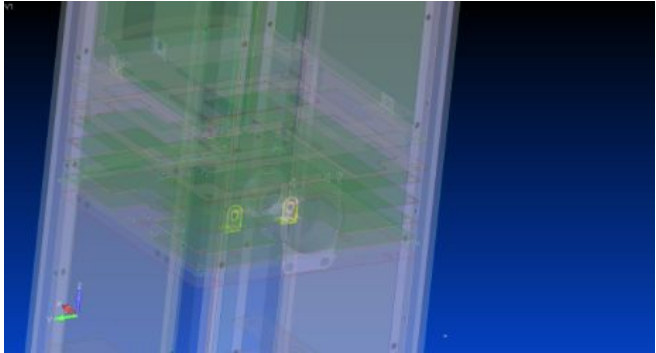
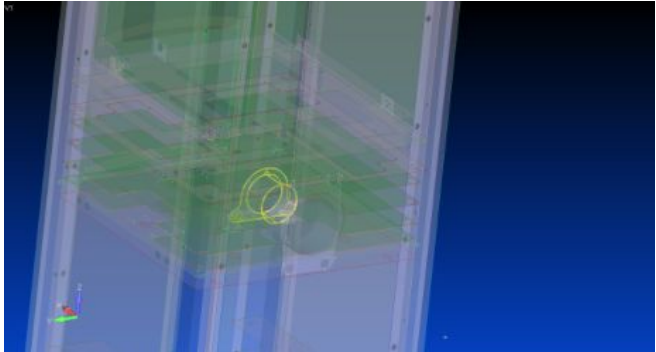
U-frame Y-plus	2.2	
Z-plus PL bottom plate	3-4	
Z-plus PL HV PCB	1.6	
Z-plus motor PCB	1.6	

Z-plus HSCOM PCB1	1.6	
Z-plus HSCOM PCB2	1.6	
Z-plus PL bottom plate	2.5-4	
Z-plus top cover	1-7	

Z-plus bottom cover	1-7	
EO bottom plate 1	4	
EO bottom plate 1	4	
Deployable hinges	3	

Deployable panel Y-plus	1-3	
Deployable panel Y-minus	1-3	
Side panel Y-plus	1	
Side panel Y-minus	1	

Side panel X-plus	1	
Side panel X-minus	1	
IFA	0.5	
Coating experiment holder	2	

ST fixtures	2	
ST optics holder	2.4-5	
ST baffle	2-4	